ISSN 1949-8470 (online)

World Journal of *Radiology*

World J Radiol 2024 April 28; 16(4): 72-108

Published by Baishideng Publishing Group Inc

World Journal of Radiology

Contents

Monthly Volume 16 Number 4 April 28, 2024

MINIREVIEWS

ORIGINAL ARTICLE

Observational Study

World Journal of Radiology

Monthly Volume 16 Number 4 April 28, 2024

Contents

ABOUT COVER

Editorial Board Member of *World Journal of Radiology*, Xiang-Ke Niu, MD, PhD, Associate Professor, Associate Chief, Department of Interventional Radiology, The Affiliated Hospital of Chengdu University, Chengdu 610081, Sichuang Province, China. niu19850519@163.com

AIMS AND SCOPE

The primary aim of *World Journal of Radiology* (*WJR*, *World J Radiol*) is to provide scholars and readers from various fields of radiology with a platform to publish high-quality basic and clinical research articles and communicate their research findings online.

WJR mainly publishes articles reporting research results and findings obtained in the field of radiology and covering a wide range of topics including state of the art information on cardiopulmonary imaging, gastrointestinal imaging, genitourinary imaging, musculoskeletal imaging, neuroradiology/head and neck imaging, nuclear medicine and molecular imaging, pediatric imaging, vascular and interventional radiology, and women's imaging.

INDEXING/ABSTRACTING

The *WJR* is now abstracted and indexed in PubMed, PubMed Central, Emerging Sources Citation Index (Web of Science), Reference Citation Analysis, China Science and Technology Journal Database, and Superstar Journals Database. The 2023 Edition of Journal Citation Reports® cites the 2022 impact factor (IF) for *WJR* as 2.5; IF without journal self cites: 2.3; 5-year IF: 2.5; Journal Citation Indicator: 0.54.

RESPONSIBLE EDITORS FOR THIS ISSUE

NAME OF JOURNAL
World Journal of Radiology

ISSN
ISSN 1949-8470 (online)

LAUNCH DATE
January 31, 2009

FREQUENCY
Monthly

EDITORS-IN-CHIEF
Thomas J Vogl

EDITORIAL BOARD MEMBERS
https://www.wjgnet.com/1949-8470/editorialboard.htm

PUBLICATION DATE
April 28, 2024

INSTRUCTIONS TO AUTHORS
https://www.wjgnet.com/bpg/gerinfo/204

GUIDELINES FOR ETHICS DOCUMENTS
https://www.wjgnet.com/bpg/GerInfo/287

GUIDELINES FOR NON-NATIVE SPEAKERS OF ENGLISH
https://www.wjgnet.com/bpg/gerinfo/240

PUBLICATION ETHICS
https://www.wjgnet.com/bpg/GerInfo/288

PUBLICATION MISCONDUCT
https://www.wjgnet.com/bpg/gerinfo/208

ARTICLE PROCESSING CHARGE
https://www.wjgnet.com/bpg/gerinfo/242

STEPS FOR SUBMITTING MANUSCRIPTS
https://www.wjgnet.com/bpg/GerInfo/239

ONLINE SUBMISSION
https://www.f6publishing.com

World Journal of Radiology

Submit a Manuscript: https://www.f6publishing.com

World J Radiol 2024 April 28; 16(4): 72-81

DOI: 10.4329/wjr.v16.i4.72

ISSN 1949-8470 (online)

MINIREVIEWS

Endoscopic ultrasound-guided tissue acquisition for the diagnosis of focal liver lesion

Alina Tantău, Cosmina Sutac, Anamaria Pop, Marcel Tantău

Specialty type: Gastroenterology and hepatology

Provenance and peer review: Invited article; Externally peer reviewed.

Peer-review model: Single blind

Peer-review report's scientific quality classification

Grade A (Excellent): 0
Grade B (Very good): 0
Grade C (Good): C
Grade D (Fair): 0
Grade E (Poor): 0

P-Reviewer: Mokni M, Tunisia

Received: January 31, 2024
Peer-review started: January 31, 2024
First decision: February 28, 2024
Revised: March 12, 2024
Accepted: March 21, 2024
Article in press: March 21, 2024
Published online: April 28, 2024

Alina Tantău, Department of Internal Medicine and Gastroenterology, "Iuliu Hatieganu" University of Medicine and Pharmacy, The 4th Medical Clinic CF Hospital, Cluj-Napoca 400012, Cluj, Romania

Cosmina Sutac, Department of Gastroenterology, "Prof. Dr. Octavian Fodor", Regional Institute of Gastroenterology and Hepatology, Cluj-Napoca 400162, Cluj, Romania

Anamaria Pop, Department of Gastroenterology and Hepatology, Gastroenterology and Hepatology Medical Center, Digenio Hospital, Cluj-Napoca 400058, Cluj, Romania

Marcel Tantău, Department of Internal Medicine and Gastroenterology, "Iuliu Hatieganu" University of Medicine and Pharmacy, "Prof. Dr. Octavian Fodor", Regional Institute of Gastroenterology and Hepatology, Cluj-Napoca 400162, Cluj, Romania

Corresponding author: Anamaria Pop, MD, Doctor, Department of Gastroenterology and Hepatology, Gastroenterology and Hepatology Medical Center, Digenio Hospital, 2 Portelanului Street, Cluj-Napoca 400058, Cluj, Romania. anamaria.pop09@yahoo.com

Abstract

In patients with liver tumors, the histopathology examination can assist in diagnosis, staging, prognosis, and therapeutic management strategy. Endoscopic ultrasound (EUS)-guided tissue acquisition using fine needle aspiration (FNA) or more newly fine needle biopsy (FNB) is a well-developed technique in order to evaluate and differentiate the liver masses. The goal of the EUS-FNA or EUS-FNB is to provide an accurate sample for a histopathology examination. Therefore, malignant tumors such as hepatocarcinoma, cholangiocarcinoma and liver metastasis or benign tumors such as liver adenoma, focal hyperplastic nodular tumors and cystic lesions can be accurately diagnosed using EUS-guided tissue acquisition. EUS-FNB using 19 or 22 Ga needle provide longer samples and a higher diagnostic accuracy in patients with liver masses when compared with EUS-FNA. Few data are available on the diagnostic accuracy of EUS-FNB when compared with percutaneously, ultrasound, computer tomography or transjugulary-guided liver biopsies. This review will discuss the EUS-guided tissue acquisition options in patients with liver tumors and its efficacy and safety in providing accurate samples. The results of the last studies comparing EUS-guided liver biopsy with other conventional techniques are presented. The EUS-guided tissue acquisition using FNB can be a suitable technique in suspected liver lesions in order to provide an accurate histopathology diagnosis, especially for those who

require endoscopy.

Key Words: Endoscopic ultrasound-guided liver biopsy; Liver tissue acquisition; Fine-needle aspiration; Fine-needle biopsy; Liver tumors; Focal liver lesions

Core Tip: Endoscopic ultrasound (EUS) guided tissue acquisition with fine needle aspiration or biopsy needles are an effective and safe approach to obtain liver samples. In this review our goal is to discuss the EUS-guided tissue acquisition options in patients with liver tumors and its efficacy and safety in providing accurate samples. The results of the last studies comparing EUS-guided liver biopsy with other conventional techniques are presented.

Citation: Tantău A, Sutac C, Pop A, Tantău M. Endoscopic ultrasound-guided tissue acquisition for the diagnosis of focal liver lesion. *World J Radiol* 2024; 16(4): 72-81
URL: https://www.wjgnet.com/1949-8470/full/v16/i4/72.htm
DOI: https://dx.doi.org/10.4329/wjr.v16.i4.72

INTRODUCTION

In patients with liver tumors, the histopathology examination can help in diagnosis, staging, prognosis, and therapeutic management strategy. The gold standard for diagnosis of liver tumors is liver biopsy (LB). Transjugular (TJ) and percutaneous (PC) approaches are the most common techniques for LB[1-3].

Endoscopic ultrasound (EUS)-guided tissue acquisition (EUS-TA) using fine needle aspiration (FNA) or more recently fine needle biopsy (FNB), is a well-developed technique in order to evaluate and differentiate the liver masses. The goal of the EUS-TA is to provide an accurate sample for a histopathology examination[4]. The common indication for EUS-guided FNA (EUS-FNA) is to obtain cytology or histology from primary or metastatic malignancy[5].

Nguyen *et al*[6] reported the utility of EUS-FNA in histological examination of focal liver lesions. In the last two decades there were numerous studies that emphasized the role of EUS-LB in the diagnosis of hepatic malignancies such as hepatocarcinoma carcinoma (HCC), cholangiocarcinoma (CCA), and liver metastasis[7-17] (Table 1).

Furthermore, EUS-LB seems to be efficient in providing a high diagnostic accuracy even in benign liver lesions or diffuse liver conditions[18-24].

In the majority of EUS-FNA studies where 19 gauge (G) or 22 G needles were used, the diagnostic yield of focal liver lesions vary from 80% to 90%[6-10,14-16]. However, EUS-FNB using 19 G or 22 G needles provide longer samples and a higher diagnostic accuracy in patients with liver masses when compared with EUS-FNA[11-13,15,17].

Recent data are available on the diagnostic accuracy of EUS-FNB when compared with PC, ultrasonography (US), computer tomography (CT), or TJ-guided liver biopsies[25-30]. In the last studies the yield of EUS-LB and PC or TJ liver sampling was compared. Specimen accuracy and diagnostic yield are at least comparable between those three techniques, ranging from 90% to 100%[25-30].

In this review we intent to explore and discuss the studies from the last decade regarding EUS-TA options in patients with liver tumors. Furthermore, we assessed the efficacy and safety of EUS-FNA and EUS-FNB from liver masses in providing an accurate diagnostic.

ENDOSCOPIC ULTRASOUND LIVER ASSESSING

EUS has multiple advantages in the evaluation of the liver and its focal or diffuse conditions. Both the liver lobes and liver hilum can be accurately evaluated from the stomach and bulb using the EUS approach due to the close position of the transducer[5]. EUS is an adjuvant method to magnetic resonance imaging (MRI) and CT in detecting and characterizing liver tumors and is superior to CT in diagnosing liver lesions located in the left lobe or smaller than 10 mm in diameter[5,31,32].

Tissue acquisition under EUS guidance (FNA) or FNB is a helpful technique in the diagnosis of focal liver lesions, perihepatic adenopathy and in the evaluation of biliary tract disease. In contrast with other techniques, liver EUS has some advantages as targeting the caudal lobe, avoiding the biliary tree and vessels during puncture. It is a real-time technique and the perihepatic lymph nodes and portal vein thrombosis can be targeted in the same session[32].

The malignant tumors such as HCC, CCA, and liver metastasis or benign tumors such as liver adenoma, focal hyperplastic nodular tumors and cystic lesions can be accurately diagnosed using EUS-TA[4,5,31,32] (Figure 1).

There are various factors which can influence the diagnostic yield of EUS or EUS-LB: The features of the liver lesions (localization: Caudal or left lobe or right lobe, size and echogenicity), the examiner experience, the type of the needle, the number of passes, the aspiration /biopsy technique (stylet and suction), the presence of the cytopathologist in the

Table 1 Literature data: Diagnostic accuracy, success rate, adverse events, and complications of endoscopic ultrasound guided biopsies for liver lesions

Ref.	Study design	Lesions/patients, *n*	Results	Succes rate, adverse events
DeWitt *et al* [9], 2003	Large study	77 SLT; FNA	77 liver specimens, 25 benign (33%); 45 malignant (58%), and 7 nondiagnostic (9%)	Sensitivity for the diagnosis of malignancy ranged from 82% to 94%
Lee *et al* [11], 2015	Prospective study	21 SLT with nonconclusive diagnosis after percutaneous biopsy	21 lesions were malignant	Diagnostic accuracy-85.7% (diagnosis of malignancy in 19 cases)
Oh *et al*[12], 2017	Study liver masses	47 patients with liver masses FNA; 24 left lobe (51.1%); 13 right lobe (27.7%); 10 both lobe (21.3%); size of lesion, median, 26 mm (15-37); number of needles passes 3	9 benign (19.15%); 38 malignant (80.95%); technical success 97.9%; EUS-FNA was diagnostic in 38 of 42 patients (90.5%); technical success similar in both lobs (100% left lobe *vs* 94.1% right lobe)	Adequate specimen higher in left lobe (93.3% *vs* 82.4%); diagnostic accuracy not different between lobes (89.3% *vs* 92.9%); no complications
Temnykh *et al*[13], 2020	Prospective study	180 solid lesions; FNB (Franseen) *vs* 183 solid lesions; FNA (acquire) 32 liver lesions (23 FNA, 9 FNB)	37.4 min (FNB) *vs* 44.9 (FNA) min; 2.9 passes FNB *vs* 3.8 passes FNA	Cytologic diagnostic yield 98.3% (FNB) *vs* 90.2% (FNA), $P = 0.003$; adverse events 1.1% (FNB) *vs* 0.5% (FNA)
Akay *et al* [14], 2021	Retrospective study	25 patients with SLT, FNA 22 G, 1 pass	16 malignancies: 7 HCC, 1 CCA, 1 adenoma, 6 metastasis, 1 GB cancer infiltration; 3 benign (3 steatosis), 3 inadequate materials	Diagnostic accuracy 86.30%, success rate 88.00% (22 patients), 94.45% aspirate sufficiency, 86.30% biopsy sufficiency rate
Chen *et al* [15], 2020	Retrospective study	34 patients with cirrhosis and suspected left lobe HCC, FNB	30 adequate biopsies specimens; 25 patients confirmed HCC, 5 benign	Se/Sp/PPV/NPV, 88.0%/100.0%/100.0%/62.5%
Chen *et al* [16], 2014	Retrospective study	4312 patients with suspected HCC with AFP under 200ng/dL FNA; 1756 underwent FNA	1590 malignant (1145 primary liver neoplasm: HCC 1067, CCA 63, HCC-CCA 8, hepatoblastoma 1, lymphoma 6, metastasis neoplasms 75), 166 benign	112 false negative, Se 92.00%, Sp 96.00%, PPV 100.00%, NPV 59.71%; overall accuracy 93.62%; complications: 4 implantation metastasis, 6 hemorrhage
Zhang *et al* [17], 2020	Retrospective study	624 malignant liver cases FNB	448 metastases(71.8%), 97 HCC (28.2%), 73 CCA, 3 HCC-CCA, 58 NET (11.7%), 24 SSC (3.8%); embryonal sarcoma, hepatoblastoma, leiomyosarcoma	30 different types of malignant tumors
Ichim *et al* [40], 2019	Prospective study	48 patients with malignant SLT FNA 22 G	47 malignancies, 1 insufficient, metastasis pancreatic ADK 26% CCA 17%	Diagnostic yield 98%, 83% from left lob, 17% from right lob, no adverse events/complications
Gheorghiu *et al*[41], 2022	Head-to-head study, prospective trial	38 SLT; 22 G FNB *vs* 22 G FNA	25 malignant lesions (14 metastases and 11 primary liver tumors); 6 benign lesions (abscesses); 7 inconclusive	Diagnostic rate for FNB-93.9%; insufficient core 4.0% (FNB) *vs* 20.0% (FNA)
Choi *et al* [65], 2017	Liver study	28 patients with SLT located in the left liver lobe FNB	KRAS mutation was analyzed	Diagnostic accuracy for malignancy 89.3%; adding KRAS diagnostic accuracy 96.4%

FNA: Fine needle aspiration; FNB: Fine needle biopsy; SLT: Solid liver tumor; HCC: Hepatocarcinoma carcinoma; CCA: Cholangiocarcinoma; GB: Gallbladder; Se: Sensibility; Sp: Specificity; PPV: Positive predictive value; NPV: Negative predicting value; AFP: Alfa feto protein; NET: Neuroendocrine tumor; ADK: Adenocarcinoma; SSC: Squamous cell carcinoma.

endoscopy room (ROSE), the preparation of the specimen for cytohistologic examination and the cytopathologist experience[33-38].

EUS-GUIDED LIVER ACQUISITION

Tru-cut needles: Mathew *et al*[21] published the first case of EUS-LB using a novel Tru-Cut (Quick-Core, Cook Medical) core biopsy needle. Later in a study by DeWitt *et al*[19], 21 patients underwent EUS-guided Tru-Cut biopsy from benign liver disease. A histology diagnosis was obtained in the majority of the cases (90%) but the standard criteria for histology assessment was not met due to the small size of samples[19]. More recently, in a large retrospective study the Tru-Cut needle was compared with a non Tru-Cut needle (ProCore needle, Cook Medical) and the results showed that the ProCore needle was easier to use and provided good tissue with fewer passes than the Tru-Cut needle[39]. Nowadays, the widespread adoption of the Tru-Cut needle is limited due to the inflexibility and the difficulty of use resulting in the manufacturers considering removing this needle from clinical practice.

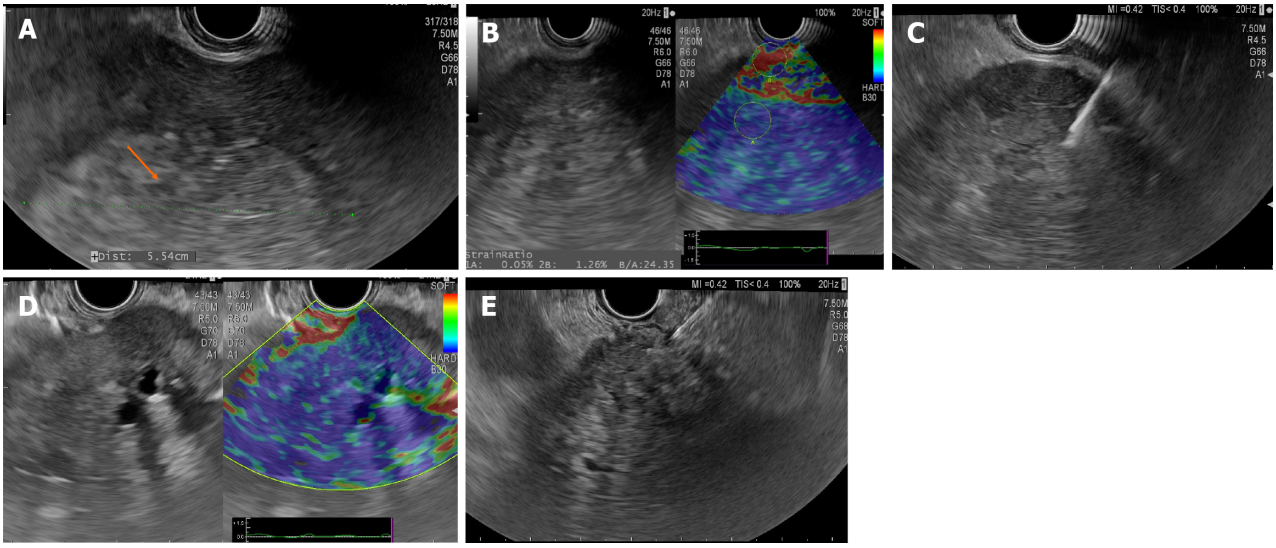

Figure 1 Endoscopic ultrasound. A and B: Endoscopic ultrasound view of a right lobe hepatocarcinoma. Large hyperechoic tumor mass with halo segments V-VIII (A), Ultrasound elastography showing high strain ration predicting malignant character of the lesion (B); C: Endoscopic ultrasound guided fine needle biopsy from a left lobe hepatocarcinoma in a patient with liver cirrhosis; D and E: Endoscopic ultrasound view of a left lobe cholangiocarcinoma. Large inhomogeneous tumor mass with intratumoral left bile duct dilatations (D); Endoscopic ultrasound guided fine needle aspiration from the tumor mass (E).

EUS-FNA FOR LIVER TUMORS

Stavropoulos *et al*[22], published in 2012, an important study which demonstrated the efficacy of a 19 G FNA in EUS-LB. Moreover, the efficacy of 19G FNA in EUS-LB was shown in a multicenter prospective study conducted by Diehl *et al*[23] in patients with elevated liver enzymes or hepatic disease. EUS-LB was performed in 110 patients and in the majority (108 patients) the specimens obtained were sufficient for a pathological diagnosis. The study demonstrated high tissue specimen lengths and portal tract counts. No differentiation in yield was detected between the right lobe, left lobes or both lobes[23].

In the last two decade, EUS-FNA has demonstrated its role in patients with liver tumors. Earlier previous studies demonstrated a sensitivity of 19G EUS-FNA for liver malignancy and ranged 75%-100% with very low morbidity and mortality[8-10]. In a large study, Dewitt *et al*[19] assessed the role of EUS-FNA in differentiation benign lesions from malignant liver lesions. From 77 liver specimens, 25 were benign, 45 were malignant, and 7 were nondiagnostic. Of the patients with malignancy identified *via* cytology, EUS-FNA changed the management in 86% of the subjects[19].

Studies from the last decade using 22 G FNA evidenced high efficacy and diagnostic accuracy for liver malignancy diagnosis[14,40,41]. In a retrospective small study conducted by Akay *et al*[14] on 25 patients with liver masses, the success rate and the diagnostic accuracy using FNA 22G and only 1 pass were evaluated. The success rate was 88.00% (22 patients). In 94.45% of cases the rate of aspirate was sufficient. The diagnostic accuracy was 86.30%. Sixty cases were malignant, 3 lesions were benign and in 3 cases the material was inadequate. The results were better, in a prospective study conducted by Ichim *et al*[40], on 48 consecutive patients; for those diagnosed with liver lesions, EUS-guided 22G FNA yielded positive results for malignancy in 47 out of 48 patients. Only one case had an inadequate sample, resulting in a diagnostic yield of 0.98. The majority of the biopsies, 83%, were from the left liver lobe and 17% from the right, with no significant difference in diagnostic accuracy between the lobes. Similar results were obtained by Gheorghiu *et al*[41].

EUS-FNB FOR LIVER TUMORS

FNB is another approach developed to enhance the histology diagnosis. In the past years, to improve the diagnostic accuracy of EUS-FNB, several core needles were developed. This approach was able to obtain histology core specimens [42,43]. The 3rd generation of EUS biopsy needles had demonstrated a better diagnostic yield compared to the first generation of FNB needles and FNA needles[44,45]. There are several types of FNB needles available for clinical practice (Acquire, ProCore, SharkCore, EchoTip, EZ shot 3, *etc*.). The available diameter of needles is 19, 20, 22 and 25 G.

EUS-FNB demonstrated a high diagnostic rate of 93.9%-100.0% with a low complication rate and a lower incidence of inadequate sample size[26,46,47]. In 2015, a prospective randomized study conducted by DeWitt *et al*[46] compared EUS-TA using two different 19 G core biopsy needles. Eighty-five patients were randomized to FNB (44 patients) and true-cut biopsy (41 patients). FNB specimens had a higher prevalence of diagnostic histology (85 % *vs* 57 %), accuracy (88 % *vs* 62%), mean total specimen length (TSL) (19.4 mm *vs* 4.3 mm), mean complete portal triads (CPTs) from liver biopsies (10.4 *vs* 1.3). Shah *et al*[26] showed a similar results in a retrospective study (n = 24) of patients with pancreatobiliary conditions and abnormal liver functional tests (LFTs) who had underwent EUS-TA with a 19 G FNB (SharkCore). A histology diagnosis was obtained in the majority of cases (96%), with a median CPT of 32.5, median TSL of 65.6 mm, and a median of two passes. Nieto *et al*[47] conducted a retrospective study on 165 patients with elevated LFTs using the wet

suction technique FNB in patients with elevated LFTs who had undergone EUS-LB. The median number of CPTs was 18, the median TSL was 60 mm.

FNA biopsy with 19 G needle is the most commonly used method for the diagnosis of liver tumors. Previous studies have revealed a better specimen, a higher diagnostic accuracy and less needle passes when EUS-FNB is used for liver masses diagnostic[11-13,15,17,48,49]. Lee *et al*[11] conducted a prospective, single center in order to assess the role of EUS-FNB of solid liver lesions following an inconclusive LB guided under abdominal US. A 25 or 22G FNB needle was used according to whether the biopsy was performed using the duodenum approach or stomach approach, respectively. EUS-FNB was able to diagnose malignant lesions in 19 of 21 cases (85.7%). Adler *et al*[49] performed a multicenter retrospective study of 200 patients undergoing EUS-FNB for solid lesions. Liver lesions were presented in only 14 patients (8 CCA and 6 liver lesions). The median passes were 3 and the rate of a core of tissue was 90%. No adverse events were detected. Chen *et al*[15] evaluated 34 patients with cirrhosis and left lobe suspected hepatocarcinoma performing EUS-FNB with 30 adequate biopsy specimens. HCC was confirmed in 25 patients and in 5 patients the lesions were benign. The sensitivity, specificity, positive predictive value (PPV) and negative predictive value (NPV) of EUS-FNB for histology diagnosis were 88.0%, 100.0%, 100.0%, respectively 62.5%[15].

The majority of studies have found that FNB with 19 G needle is better than FNB with 22 G needle in terms of length of the specimens, numbers of portal tracts and eventual histological diagnosis accuracy[26,39,48,50]. In a prospective case series of patients (n = 20) undergoing EUS-LB, Shah *et al*[50] sought differences in liver tissue acquisition obtained by wet suction technique using a 22 G FNB needle and a 19 G FNB needle from the left lobe of the liver. The mean TSL was significantly longer for the 19 G core sample *vs* the 22 G core sample: 25.2 mm and 12.7 mm respectively (P < 0.0001). The 19 G needle also resulted in a significantly higher number of CPTs (5.8 *vs* 1.7, P < 0.0001) when compared to the 22 G needle. The 19 G needle was also superior in providing an adequate and diagnostic specimens (85% *vs* 10%) and pathology samples (60% *vs* 5%) than 22 G needle. There were no adverse events in either group[50].

Interestingly, some recent studies concluded that the diameter of 19 G and 22/25 G of FNB needles seem to be similar in terms of the length of specimen and the diagnostic accuracy from focal and diffuse liver diseases[11,51]. For example, Hasan *et al*[51] conducted a single-center, prospective, open label, nonrandomized trial on 48 patients with elevated liver function test findings (8 were excluded due to biliary obstruction). The authors compared 22 G FNB with 19 G FNB in terms of the length of specimen and the diagnostic accuracy from diffuse liver diseases. Three passes were made in each of the 40 patients (total 120 passes). An adequate tissue specimen, as judged by on-site visual estimation, was obtained in 119 passes (99.2%). All 40 patients (100.0%) had adequate core tissue samples by visual estimation within the first two passes. Per patient analysis, the median TSL was 55 mm, the median CPTs was 42[51].

FNB *VS* FNA FOR LIVER TUMORS

In the case of focal liver lesions, there have been several articles published concerning the needle size or type. The rate of EUS-FNA diagnosis varied between 75% to 100% with two to three needle passes[8-10]. The latter studies have demonstrated that FNB needles are better than FNA needles in terms of tissue specimen acquisition, yield of histology accuracy and regarding time spent[26,46,47]. In a prospective study published by Temnykh *et al*[13], compared EUS-FNB in 180 patients with EUS-FNA in 183 patients with solid lesions; the number of passes was higher in the FNA group *vs* the FNB group (3.8 *vs* 2.9). The procedural time was longer in the FNA group. The yield of histology accuracy was significantly higher in the FNB group. The same results reached Iqbal *et al*[52] when two FNB needles (SharkCore, Medtronic and Acquire, Boston Scientific) and FNA needle (Echotip Cook) were compared. The diagnostic yield was much higher in the EUS-FNB group (96.0%/94.9%) than the EUS-FNA group (86.2%). No difference was reported when FNB needles were compared.

A head-to-head comparison of 22G FNA *vs* 22G FNB in the diagnosis of focal liver lesions was conducted by Gheorghiu *et al*[41]. This trial prospectively included 32 patients diagnosed with solid hepatic masses by CT scan and unsuitable for PC LB or requiring a EUS-guided sampling from both pancreas and focal liver lesions. The final diagnosis was based on EUS-FNB or EUS-FNA results in 25 patients with malignant lesions (14 metastases and 11 primary liver tumors). The remainder of the six benign lesions were abscesses. The diagnostic rate for EUS-FNB was reported to be 93.9%, with an adverse rate of 2.3%, and an insufficient core was considered to be 4% compared to 20% in the case of FNA needles. Franseen FNB needles obtained better results than Fork-tip needles. They obtained 100% diagnostic accuracy with Franseen FNB needles[41].

A small study conducted by Rodrigues-Pinto *et al*[53], on 33 patients compared the FNA with ROSE performed with a standard FNA needle with FNB with ROSE performed with a new dedicated core needle in patients with malignancies. The authors did not find any differences in terms of the diagnosis of malignancy, sensitivities, specificity, and accuracy for cancer between these two EUS sampling methods. However, FNB provided qualitative information as a degree of differentiation in malignancy, metastatic origins, and rate of proliferation. The authors concluded that when using FNB the role of the onsite cytopathologist was no longer mandatory[53].

LOCALISATION OF LIVER TUMORS: LEFT *VS* RIGHT LIVER LOBE

EUS can properly evaluate the left lobe of the liver but the latest case reports and studies have shown that even lesions located in the right lobe can be targeted[12,14,41,54].

Oh *et al*[12], reported the utility of EUS-FNA on liver masses on 47 patients (24 patients with lesions in the left lobe, 13 patients with lesions in the right lobe and 10 patients with lesions in the both lobes). The median size of the lesion was 26 mm (15-37) and three median number of needle passes were needed. Technical success was reported in 97.9% of cases. EUS-FNA was diagnostic in 38 of 42 patients (90.5%). The technical success was similar in both lobes (100.0% in the left lobe *vs* 94.1% in the right lobe) but the adequate specimen rate was statistically higher if the FNA was performed from the left lobe rather than from the right lobe (93.3% *vs* 82.4%). However, the diagnostic accuracy was similar (89.3% *vs* 92.9%, $P = 0.86$). There were no complications reported[12].

Recently, Ichim *et al*[40] included 48 patients with hepatic tumors. The authors targeted lesions from the left and right lobe (83% lesions from left lobe, 17% lesions from right lobe). In almost all patients (47 patients) the malignancy was detected and in only 1 case the material was insufficient for a proper diagnosis.

COMPARISON OF EUS-GUIDED TISSUE ACQUISITION WITH OTHER CONVETIONAL TECHNIQUES

EUS-TA were compared with other techniques such as CT, US, and TJ in terms of diagnostic accuracy of hepatic tumors. The majority of the studies found similar results between those techniques with a high diagnostic accuracy[25-30].

A recent meta-analysis conducted by Shah *et al*[24] on 12 studies which comprised 885 adults patients who underwent EUS-LB due to elevated liver function tests without biliary obstruction demonstrated the efficacy and safety of EUS-guided LB. Pineda *et al*[25] compared the liver specimens and diagnostic accuracy of LB guided-EUS with PC-LB and TJ-LB. The authors found no differences between the techniques, the EUS-LB having similar diagnostic accuracy varying between 90% to 100% with the other techniques. Similar results were obtained in a recent study conducted by Bhogal *et al* [27]. The authors compared EUS-LB, with PC-LB and TJ-LB in terms of adverse events rate, technical success, and diagnostic adequacy of the sample for histology analysis. A total of 513 patients were retrospectively included (135 EUS-LB, 287 PC-LB, and 91 TJ-LB). The indication for EUS-FNB was liver test abnormality. No difference was detected regarding adverse events between the groups. The technical success rate was 100% in each group. No statistical difference was noted in terms of diagnostic adequacy (100% in the YJ-LB group and 99% in both EUS-LB and PC-LB groups).

In a more recent study, Takano *et al*[28] compared PC-LB (16 G needle) and EUS-LB (192225 G needle) on a total of 106 patients with liver tumors (47 in the PC group and 59 in the EUS group), the authors discovered similar results in terms of sensitivity, specificity, and accuracy of the procedure (95%, 100%, and 96% in the PC group and 100%, 100%, and 100% in the EUS group) respectively. Adverse events were reported in 17% of the PC group, with a significantly lower rate reported in the EUS group (2%; $P < 0.01$)[28].

Liver biopsies for focal liver lesions conducted using EUS guidance are comparable with those guided by interventional radiology (IR). Moreover, liver biopsies performed under EUS guidance demonstrated a superior safety profile, evidenced by a notable reduction in hospital admission post-procedure compared to the conventional IR-guided method as it was demonstrated in a retrospective observational cohort study on 152 patients[29]. Shuja *et al*[29] sought to compare EUS-LB, TJ-LB and PC-LB. The PC-LB technique was subdivided into US and CT guided LB. Average needles sizes were the following: TJ 20G, EUS 19G, PC 18G. Despite an equal number of biopsy pass attempts (median 3 passes), specimen taken *via* EUS guidance produced significantly more tissue in terms of TSL, compared to IR-guided procedures (46 mm *vs* 36 mm, $P \leq 0.01$). However, the overall tissue yield in terms of CPTs was higher in IR-guided procedures (13.6 *vs* 10.8, $P \leq 0.01$). The overall complication rate from IR-LB was higher compared to EUS-LB (7% *vs* 0%, $P \leq 0.05$)[29].

A recent study conducted by Patel *et al*[30], indicates that performing EUS-LB by new 19 G FNB needles outperforms PC-LB and TJ-LB in numerous respects. The authors, included a total of 92 patients in this study (52 patients underwent 53 EUS-LB). These were compared to 20 patients that underwent PC-LB and 20 patients that underwent TJ-LB. EUS-LB was performed from both lobes (31; 58.5%) and one lobe (22; 41.5%) while PC-LB and TJ-LB were performed from one lobe. Significantly fewer needle passes, were performed in EUS-LB group compared to TJ-LB group. EUS-LB produced a greater number of CPTs compared to PC-LB. The mean TSL was higher in EUS-LB than both PC-LB and TJ-LB. The recovery after EUS-LB was significantly shorter compared to the other procedures. Post procedure pain refractory to narcotics and requiring admission was similar among all 3 groups (EUS, 5.7%; PC, 5.0%; TJ, 5.0%)[30].

The latter findings underscore the high efficiency and safety profile of EUS-guided liver biopsies, advocating its widespread adoption in patients who require a LB in conjunction with an endoscopic procedure.

LIVER TUMORS

Malignant liver tumors

Metastasis are the most frequent malignant liver tumors detected by diverse imagistic techniques. The liver is a common site for metastases, especially from malignant epithelial tumors in sites drained by the portal venous system (gastrointestinal tract, pancreas). For primary neoplasms, HCC is usually suspected in cirrhotic liver, while CCA is more common in non-cirrhotic liver[55].

HCC

In cirrhotic patients with hepatic nodules larger than 10 mm, the experts recommend 2 or more imaging techniques for HCC diagnosis[56,57]. In suspected lesions smaller than 20 mm, a histology conformation is mandatory. The European guidelines recommend histology confirmations only in patients with nodules smaller than 20 mm with a value of alpha

feto-protein under 200 ng/mL and without a pathognomonic vascularization pattern at imaging assessment[56,57].

Although liver imaging is typically accurate, in some cases distinguishing between hepatocellular neoplasms and regenerative or dysplastic nodules can be challenging and necessitates histology assessment. Tissue samples can be obtained *via* ultrasound or CT-guided PC biopsies, or through EUS-guided biopsies[5,7,8].

Aside of tissue acquisition, the EUS has a lot of advantages when it is performed in patients with cirrhosis. In the same session, it can assess the portal or biliary tree and it can detect focal lesions, even smaller than 10 mm diameter. Moreover, it can be associated with some additional methods such as contrast enhancement and elastography for better characterization of the tumoral lesions. Contrast enhancement EUS can provide information regarding vascular behavior of focal tumors. HCC has an hyperenhancement behavior with a fast wash-out pattern. Elastography with shear wave assess the rigidity of the liver and can provide a histogram and by adding strain ratio calculation it can be helpful in assessing the rigidity and malignancy of the tumor[5,8,58-61].

In recent literature there are some studies which have assessed the efficacy of either EUS-FNA or EUS-FNB on cirrhotic patients with suspected HCC[15,16]. Chen *et al*[15] evaluated 34 patients with cirrhosis and left lobe suspected hepatocarcinoma using EUS-FNA. HCC was confirmed in 25 patients, the remaining lesions were benign. The sensitivity was 88%. Chen *et al*[16] conducted a large retrospective study on 4312 patients with suspected HCC and serum AFP under 200 ng/dL. From 1756 who underwent EUS-FNA, in 1590 cases the malignancy was confirmed (1145 primary liver neoplasms: HCC in 1067 cases, CCA in 63 patients, HCC with CCA in 8 cases and 75 metastasis neoplasms) and in 166 cases the specimens were benign. One hundred and twelve punctures were false negative. The overall accuracy of EUS-FNA was 93.62% without any differences between tumors size under 20 mm or larger than 20mm in terms of sensitivity, specificity, PPV, and NPV, which showed the advantage of FNA in the diagnostic efficacy in small hepatic lesions. The hemorrhage was present in 6 patients but in 3 patients it was fatal. Implantation metastasis was present in four cases (0.23%)[16] (Table 1).

LIVER METASTASIS

Transabdominal US, CT scan, and MRI are the diagnostic tests of choice to detect hepatic lesions suspicious of metastasis [62,63]. Unfortunately, the detection rate of small liver tumors less than 10 mm is low. Liver EUS evaluation is an additional technique to CT and RMN in order to diagnose focal liver masses, having a better detection rate for small lesions[60].

The liver is a common site for metastases from the digestive tract or pancreas. Other common primary sites include the lung, breast, kidney, and melanoma. Sarcomas, sarcomatoid carcinomas and lymphomas may also involve the liver[62,63].

In cases with liver metastasis of unknown origin, EUS is the best method. An endoscopy with an evaluation of the esophagus, stomach and duodenum is performed in conjunction with an EUS assessing the pancreas, CBP, gallbladder, adrenal cortex, retroperitoneal space, mediastinum, and liver[60].

Recently, Fujii-Lau *et al*[64] in order to differentiate benign and malignant metastatic liver tumors reported 7 EUS-derived features. The authors obtained a modest inter-observer agreement among experts with a positive predictive value of 88% and an area under the curve of 0.92. The EUS features proposed by Fujii-Lau *et al*[64] are not suitable for HCC.

Zhang *et al*[17] retrospectively evaluated 624 malignant cases. The authors performed EUS-FNB and detected 448 cases of metastasis (71.8%). The majority were adenocarcinoma from the gastrointestinal tract and pancreas. The lower frequency of metastasis was from the thyroid, prostate, and adrenal cortex. In 24 cases metastasis from squamous cell carcinoma (3.8%) was detected. The were rare cases of embryonal sarcoma, hepatoblastoma, and leiomyosarcoma[17]. EUS-FNA has also good results on liver malignant lesions in terms of histology diagnosis. For example, in a study conducted on 30 patients, in 97% of patients, the results of EUS-FNA were adequate for diagnosis, with 27/30 (90%) being malignant and 2/30 (7%) being benign[40]. However, in suspected malignant focal liver lesions, EUS-FNB is the preferred method for tissue acquisition providing accurate specimens for immunohistochemistry or genetic tests[59]. For example, a study conducted by Choi *et al*[65] performed an EUS-FNB from solid liver masses from the left lobe and analyzed the KRAS mutation by the PNA-PCR clamping method and the NGS method. Adding the results of KRAS mutation analysis to the histopathology evaluation, the overall diagnostic accuracy of EUS-guided tissue sampling was high (96.4%).

CONCLUSION

In the light of previous and recent results regarding the efficacy of EUS-guided liver FNA and with the further support of new FNB needles, we consider that the EUS-TA is an optimal tool for an accurate histology diagnosis. EUS-LB has comparable efficacy with conventional techniques but with fewer adverse events and a shorter duration of hospitalization. The EUS-TA can be a suitable technique in patients with suspected liver lesions in order to provide an accurate histopathology diagnosis, especially for those who need endoscopy.

FOOTNOTES

Author contributions: Tantău A wrote the paper and provided the endoscopic ultrasound imagines from her personal collection; Sutac C and Pop A collected the data and draft the paper; Tantău M revised the paper; and all authors contributed with expert opinion on the

concept paper and critically revising the article, and approved the final article version to be published.

Conflict-of-interest statement: The authors declare no conflicts of interest.

Country/Territory of origin: Romania

ORCID number: Alina Tantău 0000-0001-5975-0779; Anamaria Pop 0000-0002-4884-8145; Marcel Tantău 0000-0002-7749-0007.

S-Editor: Chen YL
L-Editor: A
P-Editor: Zhao S

REFERENCES

1 **Rockey DC**, Caldwell SH, Goodman ZD, Nelson RC, Smith AD; American Association for the Study of Liver Diseases. Liver biopsy. *Hepatology* 2009; **49**: 1017-1044 [PMID: 19243014 DOI: 10.1002/hep.22742]
2 **Behrens G**, Ferral H. Transjugular liver biopsy. *Semin Intervent Radiol* 2012; **29**: 111-117 [PMID: 23729981 DOI: 10.1055/s-0032-1312572]
3 **Bravo AA**, Sheth SG, Chopra S. Liver biopsy. *N Engl J Med* 2001; **344**: 495-500 [PMID: 11172192 DOI: 10.15722/jds.15.10.201710.15]
4 **Parekh PJ**, Majithia R, Diehl DL, Baron TH. Endoscopic ultrasound-guided liver biopsy. *Endosc Ultrasound* 2015; **4**: 85-91 [PMID: 26020041 DOI: 10.4103/2303-9027.156711]
5 **Bissonnette J**, Paquin S, Sahai A, Pomier-Layrargues G. Usefulness of endoscopic ultrasonography in hepatology. *Can J Gastroenterol* 2011; **25**: 621-625 [PMID: 22059170 DOI: 10.1155/2011/367643]
6 **Nguyen P**, Feng JC, Chang KJ. Endoscopic ultrasound (EUS) and EUS-guided fine-needle aspiration (FNA) of liver lesions. *Gastrointest Endosc* 1999; **50**: 357-361 [PMID: 10462656 DOI: 10.1053/ge.1999.v50.97208]
7 **Maheshwari A**, Kantsevoy S, Jagannath S, Thuluvath PJ. Endoscopic ultrasound and fine-needle aspiration for the diagnosis of hepatocellular carcinoma. *Clin Liver Dis* 2010; **14**: 325-332 [PMID: 20682238 DOI: 10.1016/j.cld.2010.03.014]
8 **Awad SS**, Fagan S, Abudayyeh S, Karim N, Berger DH, Ayub K. Preoperative evaluation of hepatic lesions for the staging of hepatocellular and metastatic liver carcinoma using endoscopic ultrasonography. *Am J Surg* 2002; **184**: 601-4; discussion 604 [PMID: 12488184 DOI: 10.1016/s0002-9610(02)01092-9]
9 **DeWitt J**, LeBlanc J, McHenry L, Ciaccia D, Imperiale T, Chappo J, Cramer H, McGreevy K, Chriswell M, Sherman S. Endoscopic ultrasound-guided fine needle aspiration cytology of solid liver lesions: a large single-center experience. *Am J Gastroenterol* 2003; **98**: 1976-1981 [PMID: 14499774 DOI: 10.1111/j.1572-0241.2003.07638.x]
10 **Hollerbach S**, Willert J, Topalidis T, Reiser M, Schmiegel W. Endoscopic ultrasound-guided fine-needle aspiration biopsy of liver lesions: histological and cytological assessment. *Endoscopy* 2003; **35**: 743-749 [PMID: 12929021 DOI: 10.1055/s-2003-41593]
11 **Lee YN**, Moon JH, Kim HK, Choi HJ, Choi MH, Kim DC, Lee TH, Cha SW, Kim SG, Kim YS. Usefulness of endoscopic ultrasound-guided sampling using core biopsy needle as a percutaneous biopsy rescue for diagnosis of solid liver mass: Combined histological-cytological analysis. *J Gastroenterol Hepatol* 2015; **30**: 1161-1166 [PMID: 25684303 DOI: 10.1111/jgh.12922]
12 **Oh D**, Seo DW, Hong SM, Jun JH, Song TJ, Park DH, Son BK, Lee SS, Lee SK, Kim MH. The usefulness of contrast-enhanced harmonic EUS-guided fine-needle aspiration for evaluation of hepatic lesions (with video). *Gastrointest Endosc* 2018; **88**: 495-501 [PMID: 29859228 DOI: 10.1016/j.gie.2018.05.019]
13 **Temnykh LM**, Rahal MA, Zia Z, Al-Haddad MA. An exclusive fine-needle biopsy approach to sampling solid lesions under EUS guidance: a prospective cohort study. *Gastroenterol Rep (Oxf)* 2020; **8**: 349-354 [PMID: 33163189 DOI: 10.1093/gastro/goaa012]
14 **Akay E**, Atasoy D, Altınkaya E, Koç A, Ertan T, Karaman H, Caglar E. Endoscopic Ultrasound-Guided Fine Needle Aspiration Using a 22-G Needle for Hepatic Lesions: Single-Center Experience. *Clin Endosc* 2021; **54**: 404-412 [PMID: 33291191 DOI: 10.5946/ce.2020.065]
15 **Chen F**, Bao H, Deng Z, Zhao Q, Tian G, Jiang TA. Endoscopic ultrasound-guided sampling using core biopsy needle for diagnosis of left-lobe hepatocellular carcinoma in patients with underlying cirrhosis. *J Cancer Res Ther* 2020; **16**: 1100-1105 [PMID: 33004754 DOI: 10.4103/jcrt.JCRT_723_19]
16 **Chen QW**, Cheng CS, Chen H, Ning ZY, Tang SF, Zhang X, Zhu XY, Vargulick S, Shen YH, Hua YQ, Xie J, Shi WD, Gao HF, Xu LT, Feng LY, Lin JH, Chen Z, Liu LM, Ping B, Meng ZQ. Effectiveness and complications of ultrasound guided fine needle aspiration for primary liver cancer in a Chinese population with serum α-fetoprotein levels ≤200 ng/ml--a study based on 4,312 patients. *PLoS One* 2014; **9**: e101536 [PMID: 25170868 DOI: 10.1371/journal.pone.0101536]
17 **Zhang L**, Cai Z, Rodriguez J, Zhang S, Thomas J, Zhu H. Fine needle biopsy of malignant tumors of the liver: a retrospective study of 624 cases from a single institution experience. *Diagn Pathol* 2020; **15**: 43 [PMID: 32375822 DOI: 10.1186/s13000-020-00965-5]
18 **Wiersema MJ**, Levy MJ, Harewood GC, Vazquez-Sequeiros E, Jondal ML, Wiersema LM. Initial experience with EUS-guided trucut needle biopsies of perigastric organs. *Gastrointest Endosc* 2002; **56**: 275-278 [PMID: 12145612 DOI: 10.1016/s0016-5107(02)70193-4]
19 **Dewitt J**, McGreevy K, Cummings O, Sherman S, Leblanc JK, McHenry L, Al-Haddad M, Chalasani N. Initial experience with EUS-guided Tru-cut biopsy of benign liver disease. *Gastrointest Endosc* 2009; **69**: 535-542 [PMID: 19231495 DOI: 10.1016/j.gie.2008.09.056]
20 **Gleeson FC**, Clayton AC, Zhang L, Clain JE, Gores GJ, Rajan E, Smyrk TC, Topazian MD, Wang KK, Wiersema MJ, Levy MJ. Adequacy of endoscopic ultrasound core needle biopsy specimen of nonmalignant hepatic parenchymal disease. *Clin Gastroenterol Hepatol* 2008; **6**: 1437-1440 [PMID: 19081532 DOI: 10.1016/j.cgh.2008.07.015]
21 **Mathew A**. EUS-guided routine liver biopsy in selected patients. *Am J Gastroenterol* 2007; **102**: 2354-2355 [PMID: 17897349 DOI:

10.1111/j.1572-0241.2007.01353_7.x]
22 **Stavropoulos SN**, Im GY, Jlayer Z, Harris MD, Pitea TC, Turi GK, Malet PF, Friedel DM, Grendell JH. High yield of same-session EUS-guided liver biopsy by 19-gauge FNA needle in patients undergoing EUS to exclude biliary obstruction. *Gastrointest Endosc* 2012; **75**: 310-318 [PMID: 22248599 DOI: 10.1016/j.gie.2011.09.043]
23 **Diehl DL**, Johal AS, Khara HS, Stavropoulos SN, Al-Haddad M, Ramesh J, Varadarajulu S, Aslanian H, Gordon SR, Shieh FK, Pineda-Bonilla JJ, Dunkelberger T, Gondim DD, Chen EZ. Endoscopic ultrasound-guided liver biopsy: a multicenter experience. *Endosc Int Open* 2015; **3**: E210-E215 [PMID: 26171433 DOI: 10.1055/s-0034-1391412]
24 **Shah AR**, Al-Hanayneh M, Chowdhry M, Bilal M, Singh S. Endoscopic ultrasound guided liver biopsy for parenchymal liver disease. *World J Hepatol* 2019; **11**: 335-343 [PMID: 31114638 DOI: 10.4254/wjh.v11.i4.335]
25 **Pineda JJ**, Diehl DL, Miao CL, Johal AS, Khara HS, Bhanushali A, Chen EZ. EUS-guided liver biopsy provides diagnostic samples comparable with those *via* the percutaneous or transjugular route. *Gastrointest Endosc* 2016; **83**: 360-365 [PMID: 26301407 DOI: 10.1016/j.gie.2015.08.025]
26 **Shah ND**, Sasatomi E, Baron TH. Endoscopic Ultrasound-guided Parenchymal Liver Biopsy: Single Center Experience of a New Dedicated Core Needle. *Clin Gastroenterol Hepatol* 2017; **15**: 784-786 [PMID: 28126424 DOI: 10.1016/j.cgh.2017.01.011]
27 **Bhogal N**, Lamb B, Arbeiter B, Malik S, Sayles H, Lazenby AJ, Chandan S, Dhaliwal A, Singh S, Bhat I. Safety and adequacy of endoscopic ultrasound-guided random liver biopsy in comparison with transjugular and percutaneous approaches. *Endosc Int Open* 2020; **8**: E1850-E1854 [PMID: 33269320 DOI: 10.1055/a-1274-9763]
28 **Takano Y**, Noda J, Yamawaki M, Azami T, Kobayashi T, Niiya F, Maruoka N, Norose T, Ohike N, Wakabayashi T, Matsuo K, Tanaka K, Nagahama M. Comparative Study of an Ultrasound-guided Percutaneous Biopsy and Endoscopic Ultrasound-guided Fine-needle Aspiration for Liver Tumors. *Intern Med* 2021; **60**: 1657-1664 [PMID: 34078770 DOI: 10.2169/internalmedicine.6183-20]
29 **Shuja A**, Alkhasawneh A, Fialho A, Shukri A, Harris C, Smotherman C, Malespin M, de Melo SW Jr. Comparison of EUS-guided versus percutaneous and transjugular approaches for the performance of liver biopsies. *Dig Liver Dis* 2019; **51**: 826-830 [PMID: 30755347 DOI: 10.1016/j.dld.2019.01.006]
30 **Patel HK**, Therapondos G, Galliano G, Romero R, Evans J, Cohen A, Mubarak MF, Shah JN, El Chafic AH. Endoscopic Ultrasound-Guided Liver Biopsy Using Newer 19-G Fine Needle Biopsy Needles Compared to Percutaneous and Transjugular Liver Biopsy: A Tertiary Center Experience. *Tech Innova Gastrointest Endosc* 2022; **24**: 127-135 [DOI: 10.1016/j.tige.2021.11.009]
31 **Saraireh HA**, Bilal M, Singh S. Role of endoscopic ultrasound in liver disease: Where do we stand in 2017? *World J Hepatol* 2017; **9**: 1013-1021 [PMID: 28932347 DOI: 10.4254/wjh.v9.i24.1013]
32 **Diehl DL**. Endoscopic Ultrasound-guided Liver Biopsy. *Gastrointest Endosc Clin N Am* 2019; **29**: 173-186 [PMID: 30846147 DOI: 10.1016/j.giec.2018.11.002]
33 **Mohan BP**, Shakhatreh M, Garg R, Ponnada S, Adler DG. Efficacy and safety of EUS-guided liver biopsy: a systematic review and meta-analysis. *Gastrointest Endosc* 2019; **89**: 238-246.e3 [PMID: 30389469 DOI: 10.1016/j.gie.2018.10.018]
34 **Hawes RH**. The evolution of endoscopic ultrasound: improved imaging, higher accuracy for fine needle aspiration and the reality of endoscopic ultrasound-guided interventions. *Curr Opin Gastroenterol* 2010; **26**: 436-444 [PMID: 20703111 DOI: 10.1097/MOG.0b013e32833d1799]
35 **Erickson RA**, Sayage-Rabie L, Beissner RS. Factors predicting the number of EUS-guided fine-needle passes for diagnosis of pancreatic malignancies. *Gastrointest Endosc* 2000; **51**: 184-190 [PMID: 10650262 DOI: 10.1016/s0016-5107(00)70416-0]
36 **Logroño R**, Waxman I. Interactive role of the cytopathologist in EUS-guided fine needle aspiration: an efficient approach. *Gastrointest Endosc* 2001; **54**: 485-490 [PMID: 11577312 DOI: 10.1067/mge.2001.118445]
37 **Gleeson FC**, Kipp BR, Caudill JL, Clain JE, Clayton AC, Halling KC, Henry MR, Rajan E, Topazian MD, Wang KK, Wiersema MJ, Zhang J, Levy MJ. False positive endoscopic ultrasound fine needle aspiration cytology: incidence and risk factors. *Gut* 2010; **59**: 586-593 [PMID: 20427392 DOI: 10.1136/gut.2009.187765]
38 **Siddiqui AA**, Kowalski TE, Shahid H, O'Donnell S, Tolin J, Loren DE, Infantolino A, Hong SK, Eloubeidi MA. False-positive EUS-guided FNA cytology for solid pancreatic lesions. *Gastrointest Endosc* 2011; **74**: 535-540 [PMID: 21737075 DOI: 10.1016/j.gie.2011.04.039]
39 **Sey MS**, Al-Haddad M, Imperiale TF, McGreevy K, Lin J, DeWitt JM. EUS-guided liver biopsy for parenchymal disease: a comparison of diagnostic yield between two core biopsy needles. *Gastrointest Endosc* 2016; **83**: 347-352 [PMID: 26278654 DOI: 10.1016/j.gie.2015.08.012]
40 **Ichim VA**, Chira RI, Mircea PA. Diagnostic yield of endoscopic ultrasound-guided biopsy of focal liver lesions. *Med Pharm Rep* 2019; **92**: 15-20 [PMID: 30957081 DOI: 10.15386/cjmed-1066]
41 **Gheorghiu M**, Seicean A, Bolboacă SD, Rusu I, Seicean R, Pojoga C, Moșteanu O, Sparchez Z. Endoscopic Ultrasound-Guided Fine-Needle Biopsy versus Fine-Needle Aspiration in the Diagnosis of Focal Liver Lesions: Prospective Head-to-Head Comparison. *Diagnostics (Basel)* 2022; **12** [PMID: 36140619 DOI: 10.3390/diagnostics12092214]
42 **Iglesias-Garcia J**, Poley JW, Larghi A, Giovannini M, Petrone MC, Abdulkader I, Monges G, Costamagna G, Arcidiacono P, Biermann K, Rindi G, Bories E, Dogloni C, Bruno M, Dominguez-Muñoz JE. Feasibility and yield of a new EUS histology needle: results from a multicenter, pooled, cohort study. *Gastrointest Endosc* 2011; **73**: 1189-1196 [PMID: 21420083 DOI: 10.1016/j.gie.2011.01.053]
43 **Bang JY**, Hebert-Magee S, Trevino J, Ramesh J, Varadarajulu S. Randomized trial comparing the 22-gauge aspiration and 22-gauge biopsy needles for EUS-guided sampling of solid pancreatic mass lesions. *Gastrointest Endosc* 2012; **76**: 321-327 [PMID: 22658389 DOI: 10.1016/j.gie.2012.03.1392]
44 **Alatawi A**, Beuvon F, Grabar S, Sarah L, Chaussade S, Terris B, Barret M, Prat F. Comparison of fenestrated vs standard needles for endoscopic ultrasound-guided biopsy of solid pancreatic lesions. *Gastrointest Endosc* 2014; **79**: AB428-9 [DOI: 10.1016/j.gie.2014.02.593]
45 **Cheng B**, Zhang Y, Chen Q, Sun B, Deng Z, Shan H, Dou L, Wang J, Li Y, Yang X, Jiang T, Xu G, Wang G. Analysis of Fine-Needle Biopsy vs Fine-Needle Aspiration in Diagnosis of Pancreatic and Abdominal Masses: A Prospective, Multicenter, Randomized Controlled Trial. *Clin Gastroenterol Hepatol* 2018; **16**: 1314-1321 [PMID: 28733257 DOI: 10.1016/j.cgh.2017.07.010]
46 **DeWitt J**, Cho CM, Lin J, Al-Haddad M, Canto MI, Salamone A, Hruban RH, Messallam AA, Khashab MA. Comparison of EUS-guided tissue acquisition using two different 19-gauge core biopsy needles: a multicenter, prospective, randomized, and blinded study. *Endosc Int Open* 2015; **3**: E471-E478 [PMID: 26528504 DOI: 10.1055/s-0034-1392222]
47 **Nieto J**, Khaleel H, Challita Y, Jimenez M, Baron TH, Walters L, Hathaway K, Patel K, Lankarani A, Herman M, Holloman D, Saab S. EUS-guided fine-needle core liver biopsy sampling using a novel 19-gauge needle with modified 1-pass, 1 actuation wet suction technique. *Gastrointest Endosc* 2018; **87**: 469-475 [PMID: 28551024 DOI: 10.1016/j.gie.2017.05.013]
48 **Lee BS**, Cho CM, Jung MK, Jang JS, Bae HI. Comparison of Histologic Core Portions Acquired from a Core Biopsy Needle and a

Conventional Needle in Solid Mass Lesions: A Prospective Randomized Trial. *Gut Liver* 2017; **11**: 559-566 [PMID: 28208006 DOI: 10.5009/gnl16284]

49 **Adler DG**, Muthusamy VR, Ehrlich DS, Parasher G, Thosani NC, Chen A, Buscaglia JM, Appannagari A, Quintero E, Aslanian H, Taylor LJ, Siddiqui A. A multicenter evaluation of a new EUS core biopsy needle: Experience in 200 patients. *Endosc Ultrasound* 2019; **8**: 99-104 [PMID: 29623911 DOI: 10.4103/eus.eus_53_17]

50 **Shah RM**, Schmidt J, John E, Rastegari S, Acharya P, Kedia P. Superior Specimen and Diagnostic Accuracy with Endoscopic Ultrasound-Guided Liver Biopsies Using 19-Gauge versus 22-Gauge Core Needles. *Clin Endosc* 2021; **54**: 739-744 [PMID: 33189102 DOI: 10.5946/ce.2020.212]

51 **Hasan MK**, Kadkhodayan K, Idrisov E, Ali S, Rafiq E, Shor DBA, Abdel-Jalil A, Navaneethan U, Bang J, Varadarajulu S, Hawes R, Pernicone P. Endoscopic ultrasound-guided liver biopsy using a 22 ga fine needle endoscopy: a prospective study. *Endoscopy* 2019; **51**: 818-824 [DOI: 10.1055/a-0967-3640]

52 **Iqbal F**, Aditi A, Huang BL, Ballonado A. Diagnostic yield of a conventional endoscopic ultrasound-fine needle aspiration (EUS-FNA) and two endoscopic ultrasound-fine needle biopsy (EUS-FNB) needles: A single-center, retrospective study. *Am J Gastroenterol* 2018; **113** Suppl 3: S442 [DOI: 10.14309/00000434-201810001-00796]

53 **Rodrigues-Pinto E**, Jalaj S, Grimm IS, Baron TH. Impact of EUS-guided fine-needle biopsy sampling with a new core needle on the need for onsite cytopathologic assessment: a preliminary study. *Gastrointest Endosc* 2016; **84**: 1040-1046 [PMID: 27345131 DOI: 10.1016/j.gie.2016.06.034]

54 **Tantau A**, Zaharie T. EUS-guided fine needle biopsy for hepatocarcinoma of the right liver lobe as a rescue diagnostic technique after a negative percutaneousguided liver biopsy. *Med Ultrason* 2023; **25**: 115-116 [PMID: 36996398 DOI: 10.11152/mu-3993]

55 **Sung H**, Ferlay J, Siegel RL, Laversanne M, Soerjomataram I, Jemal A, Bray F. Global Cancer Statistics 2020: GLOBOCAN Estimates of Incidence and Mortality Worldwide for 36 Cancers in 185 Countries. *CA Cancer J Clin* 2021; **71**: 209-249 [PMID: 33538338 DOI: 10.3322/caac.21660]

56 **European Association for the Study of the Liver**. EASL Clinical Practice Guidelines: Management of hepatocellular carcinoma. *J Hepatol* 2018; **69**: 182-236 [PMID: 29628281 DOI: 10.1016/j.jhep.2018.03.019]

57 **Ducreux M**, Abou-Alfa GK, Bekaii-Saab T, Berlin J, Cervantes A, de Baere T, Eng C, Galle P, Gill S, Gruenberger T, Haustermans K, Lamarca A, Laurent-Puig P, Llovet JM, Lordick F, Macarulla T, Mukherji D, Muro K, Obermannova R, O'Connor JM, O'Reilly EM, Osterlund P, Philip P, Prager G, Ruiz-Garcia E, Sangro B, Seufferlein T, Tabernero J, Verslype C, Wasan H, Van Cutsem E. The management of hepatocellular carcinoma. Current expert opinion and recommendations derived from the 24th ESMO/World Congress on Gastrointestinal Cancer, Barcelona, 2022. *ESMO Open* 2023; **8**: 101567 [PMID: 37263081 DOI: 10.1016/j.esmoop.2023.101567]

58 **Marques S**, Carmo J, Túlio MA, Bispo M, Matos L, Chagas C. Diagnostic Performance of Real-Time Elastography in the Assessment of Advanced Fibrosis in Chronic Hepatitis C. *GE Port J Gastroenterol* 2016; **23**: 13-18 [PMID: 28868425 DOI: 10.1016/j.jpge.2015.10.008]

59 **Schulman AR**, Lin MV, Rutherford A, Chan WW, Ryou M. A Prospective Blinded Study of Endoscopic Ultrasound Elastography in Liver Disease: Towards a Virtual Biopsy. *Clin Endosc* 2018; **51**: 181-185 [PMID: 29566479 DOI: 10.5946/ce.2017.095]

60 **Kitano M**, Kamata K. Contrast-enhanced harmonic endoscopic ultrasound: Future perspectives. *Endosc Ultrasound* 2016; **5**: 351-354 [PMID: 28000625 DOI: 10.4103/2303-9027.195852]

61 **Fusaroli P**, Napoleon B, Gincul R, Lefort C, Palazzo L, Palazzo M, Kitano M, Minaga K, Caletti G, Lisotti A. The clinical impact of ultrasound contrast agents in EUS: a systematic review according to the levels of evidence. *Gastrointest Endosc* 2016; **84**: 587-596.e10 [PMID: 27311654 DOI: 10.1016/j.gie.2016.06.006]

62 **Hein E**, Albrecht A, Melzer D, Steinhöfel K, Rogalla P, Hamm B, Taupitz M. Computer-assisted diagnosis of focal liver lesions on CT images evaluation of the Perceptron algorithm. *Acad Radiol* 2005; **12**: 1205-1210 [PMID: 16112516 DOI: 10.1016/j.acra.2005.05.009]

63 **Namasivayam S**, Martin DR, Saini S. Imaging of liver metastases: MRI. *Cancer Imaging* 2007; **7**: 2-9 [PMID: 17293303 DOI: 10.1102/1470-7330.2007.0002]

64 **Fujii-Lau LL**, Abu Dayyeh BK, Bruno MJ, Chang KJ, DeWitt JM, Fockens P, Forcione D, Napoleon B, Palazzo L, Topazian MD, Wiersema MJ, Chak A, Clain JE, Faigel DO, Gleeson FC, Hawes R, Iyer PG, Rajan E, Stevens T, Wallace MB, Wang KK, Levy MJ. EUS-derived criteria for distinguishing benign from malignant metastatic solid hepatic masses. *Gastrointest Endosc* 2015; **81**: 1188-96.e1 [PMID: 25660980 DOI: 10.1016/j.gie.2014.10.035]

65 **Choi HJ**, Moon JH, Kim HK, Lee YN, Lee TH, Cha SW, Cho YD, Park SH. KRAS mutation analysis by next-generation sequencing in endoscopic ultrasound-guided sampling for solid liver masses. *J Gastroenterol Hepatol* 2017; **32**: 154-162 [PMID: 27118240 DOI: 10.1111/jgh.13423]

World Journal of Radiology

Submit a Manuscript: https://www.f6publishing.com

World J Radiol 2024 April 28; 16(4): 82-93

DOI: 10.4329/wjr.v16.i4.82

ISSN 1949-8470 (online)

ORIGINAL ARTICLE

Observational Study

Characterization of tumors of jaw: Additive value of contrast enhancement and dual-energy computed tomography

Deepak Justine Viswanathan, Ashu Seith Bhalla, Smita Manchanda, Ajoy Roychoudhury, Deepika Mishra, Asit Ranjan Mridha

Specialty type: Radiology, nuclear medicine and medical imaging

Provenance and peer review: Invited article; Externally peer reviewed.

Peer-review model: Single blind

Peer-review report's classification
Scientific Quality: Grade B
Novelty: Grade A
Creativity or Innovation: Grade A
Scientific Significance: Grade B

P-Reviewer: Zhang Z, China

Received: December 10, 2023
Revised: March 19, 2024
Accepted: April 16, 2024
Published online: April 28, 2024

Deepak Justine Viswanathan, Ashu Seith Bhalla, Smita Manchanda, Department of Radiodiagnosis and Interventional Radiology, All India Institute of Medical Sciences, New Delhi 110029, India

Ajoy Roychoudhury, Department of Oral and Maxillofacial Surgery, All India Institute of Medical Sciences, New Delhi 110029, India

Deepika Mishra, Department of Oral Pathology and Microbiology, All India Institute of Medical Sciences, New Delhi 110029, India

Asit Ranjan Mridha, Department of Pathology, All India Institute of Medical Sciences, Ansari Nagar, New Delhi 110029, India

Corresponding author: Ashu Seith Bhalla, MBBS, MD, Professor, Department of Radiodiagnosis and Interventional Radiology, All India Institute of Medical Sciences, No. 71 Ansari Nagar East, New Delhi 110029, India. ashubhalla2@gmail.com

Abstract

BACKGROUND

Currently, the differentiation of jaw tumors is mainly based on the lesion's morphology rather than the enhancement characteristics, which are important in the differentiation of neoplasms across the body. There is a paucity of literature on the enhancement characteristics of jaw tumors. This is mainly because, even though computed tomography (CT) is used to evaluate these lesions, they are often imaged without intravenous contrast. This study hypothesised that the enhancement characteristics of the solid component of jaw tumors can aid in the differentiation of these lesions in addition to their morphology by dual-energy CT, therefore improving the ability to differentiate between various pathologies.

AIM

To evaluate the role of contrast enhancement and dual-energy quantitative parameters in CT in the differentiation of jaw tumors.

METHODS

Fifty-seven patients with jaw tumors underwent contrast-enhanced dual-energy CT. Morphological analysis of the tumor, including the enhancing solid component, was done, followed by quantitative analysis of iodine concentration (IC),

water concentration (WC), HU, and normalized IC. The study population was divided into four subgroups based on histopathological analysis-central giant cell granuloma (CGCG), ameloblastoma, odontogenic keratocyst (OKC), and other jaw tumors. A one-way ANOVA test for parametric variables and the Kruskal-Wallis test for non-parametric variables were used. If significant differences were found, a series of independent *t*-tests or Mann-Whitney *U* tests were used.

RESULTS

Ameloblastoma was the most common pathology (n = 20), followed by CGCG (n = 11) and OKC. CGCG showed a higher mean concentration of all quantitative parameters than ameloblastomas ($P < 0.05$). An IC threshold of 31.35 × 100 μg/cm^3 had the maximum sensitivity (81.8%) and specificity (65%). Between ameloblastomas and OKC, the former showed a higher mean concentration of all quantitative parameters ($P < 0.001$), however when comparing unilocular ameloblastomas with OKCs, the latter showed significantly higher WC. Also, ameloblastoma had a higher IC and lower WC compared to "other jaw tumors" group.

CONCLUSION

Enhancement characteristics of solid components combined with dual-energy parameters offer a more precise way to differentiate between jaw tumors.

Key Words: Jaw neoplasms; Ameloblastomas; Dual-energy computed tomography; Iodine quantification; Mandibular neoplasms; Maxillary neoplasms

Core Tip: Quantitative dual-energy computed tomography (DECT) parameters provide a reliable way of characterizing morphologically similar jaw lesions and can serve as a single modality to differentiate jaw lesions based on their appearance and material density concentrations. In addition to providing fast imaging and material decomposition algorithms at about comparable dosage equivalency as compared to traditional computed tomography, contrast-enhanced DECT can potentially alleviate the challenge of discriminating jaw lesions without a biopsy.

Citation: Viswanathan DJ, Bhalla AS, Manchanda S, Roychoudhury A, Mishra D, Mridha AR. Characterization of tumors of jaw: Additive value of contrast enhancement and dual-energy computed tomography. *World J Radiol* 2024; 16(4): 82-93
URL: https://www.wjgnet.com/1949-8470/full/v16/i4/82.htm
DOI: https://dx.doi.org/10.4329/wjr.v16.i4.82

INTRODUCTION

Various imaging modalities are available for the evaluation of jaw lesions, the most important being panoramic radiographs, computed tomography (CT), and magnetic resonance imaging. The imaging approach towards differentiation of these lesions is mainly based on the lesion's morphology, whether lytic, sclerotic, or mixed; multilocular or unilocular; expansion; and features of aggression[1,2]. Neoplasms across the body, including solid-cystic lesions, are characterized radiologically on the basis of qualitative and quantitative evaluation of the solid component of the tumor, which forms the major component in providing a differential diagnosis. However, the literature on jaw lesions does not emphasize the characteristics of solid components. This is also because, even though CT is used in the evaluation of these lesions, most often they are imaged without intravenous contrast agents, *i.e.*, using cone beam CT scanners.

Here comes the role of contrast-enhanced CT, which makes characterization of the solid component possible and gives important information about the nature and extent of a particular tumor, helping the radiologist to give a possible range of differential diagnoses. Dual-energy CT (DECT) is an innovative technique that operates based on differential attenuation of tissues when penetrated with higher (140 kVp) and lower (80/100 kVp) energy and combines the CT attenuation-based imaging with material-specific or spectral imaging[3]. This in turn gives the added advantage of characterizing lesions based on the quantitative parameters touted to be material-specific, which can further increase the diagnostic confidence with which the radiologist conveys the possible diagnoses. The hypothesis of this study is that the enhancement characteristics of the solid component of jaw tumors is important for the differentiation of these lesions and evaluation of the same in addition to its morphology by DECT, therefore, improving the ability to differentiate between various pathologies[4-6].

MATERIALS AND METHODS

This observational study was conducted prospectively from July 2020 to April 2022 after obtaining approval by the

Institutional Ethics Committee (IECPG-354/22.07.2020, RT-2/26.08.2020). The study subjects were patients who presented with complaints of swelling in the maxilla or mandible. Patients were first screened with panoramic radiographs. Those who were found to have any lytic or sclerotic lesions in the panoramic radiographs were included. Patients without histopathological confirmation, those with uncomplicated, typical benign cysts on orthopantomography (such as radicular cysts and dentigerous cysts), clinically insignificant lesions, patients who were unwilling to participate in the study, and those who were diagnosed with other infectious conditions like osteomyelitis, traumatic lesions, or primary tumors in the oral cavity invading the jaw, were excluded. After giving their full informed consent, all patients underwent a contrast-enhanced DECT. Blood investigations were done to evaluate the renal status before administering intravenous contrast agents.

The clinical information collected was patient demographic data (age and sex) through a proforma filled out by the patient, symptomatology (including swelling, pain, bleeding, fever, tooth mobility, trismus, or any other complaints), and their duration.

Contrast-enhanced DECT imaging

Data acquisitions were performed using single-source DECT in gemstone spectral imaging (GSI) mode with a fast tube voltage switching between 80 and 140 kVp (Revolution CT, GE Healthcare, Waukesha, WI, United States). Intravenous non-ionic contrast was given at 1.0 mL/kg. Routine soft tissue and bone windows were read. Standard multiplanar reconstructions and panoramic reconstructions were made. In addition, two types of images were obtained from the reconstruction of DECT imaging automatically with GSI viewer software (GE Healthcare) for each patient: The iodine-based and water-based material decomposition (MD) images (Figure 1).

Data collection

Morphological parameters: The location of the lesion was recorded according to the bone in which it was seen. The parameters evaluated for characterization were - size, aggression, expansion, margins, matrix, cortical involvement, mandibular canal status, and relation to teeth, while cortex involvement and soft tissue extension were evaluated for extent. Based on density and locularity, the lesion was broadly divided into four subgroups: Lytic unilocular, lytic multilocular, mixed lytic-sclerotic, and sclerotic (Figure 2). Sclerotic lesions were excluded from further quantitative analysis due to the paucity of measurable soft tissue.

DECT parameters: The regions of enhancement on soft tissue windows were selected in comparison to virtual non-contrast images, and an elliptical region of interest (ROI) was placed on the most enhancing parts as assessed on monochromatic (65 kev) and iodine images. The measurements included the mean value and area of measurement (mm^2). To ensure consistency, all measurements were performed three times at different image levels, and the average values were calculated. For all measurements, the size, shape, and position of the ROI were consistent between the soft tissue images and the iodine-based MD images, as confirmed using the copy-and-paste function. Lesions with at least a soft tissue component of 1 mm^2 were selected for analysis. The iodine concentration (IC) of the lesions was measured (expressed in multiples of 100 $\mu g/cm^3$) from the iodine-based MD image, and the water concentration (WC) from the water-based MD image (expressed in multiples of 1000 mg/cm^3) along with the overlay colormap to increase the assessed lesion contrast. The normalized IC (NIC) was calculated from the ratio of the measured IC of the lesion (ICL) and the IC of the ipsilateral common carotid artery (CCA) proximal to its bifurcation (ICA) *via* the insertion of two ROIs—one in the assessed lesion and the other in the CCA. In addition to the above, an analysis of the cystic component was also made in the unilocular ameloblastomas (UA) and odontogenic keratocysts (OKCs). The parameters recorded were IC and WC.

Histopathology data-gold standard: Post-biopsy, excision, or curettage, the sampled tissue specimens were reviewed by two consultant pathologists with 10 years of experience in oral pathology. Sections from routine tissue blocks were examined using hematoxylin and eosin staining. The results were documented as ameloblastoma and non-ameloblastoma, along with the individual-specific histopathological diagnosis.

Statistical analysis

The statistical analysis for this study was done using SPSS version 28.0 software. Continuous variables (age, tumor volume, quantitative DECT, and IHC parameters) were all summarized as mean ± SD, and categorical values were summarized as proportions. The comparison of the mean ± SD between the two groups was done using an independent sample *t*-test. Categorical variables (histopathology data, patient symptomatology, and morphological parameters) were summarized as percentages. A comparison of proportions between the two groups was done using the chi-square test. Since we compared more than two independent groups for the analysis of DECT quantitative parameters, a one-way ANOVA test was performed for variables that showed a normal parametric distribution (mean HU at 65 kev, ICL, WCL) and a Kruskal-Wallis *H* test for non-parametric variables (NIC). If significant differences were discovered, we conducted a series of independent *t*-tests and Mann-Whitney *U* tests to determine the source of the difference. The value of $P < 0.05$ was considered statistically significant. The diagnostic performance was evaluated by calculating the area under the receiver operating characteristic curve (AUC).

The statistical methods of this study were reviewed by Mr. Hem Sati from the Department of Biostatistics, All India Institute of Medical Sciences, New Delhi.

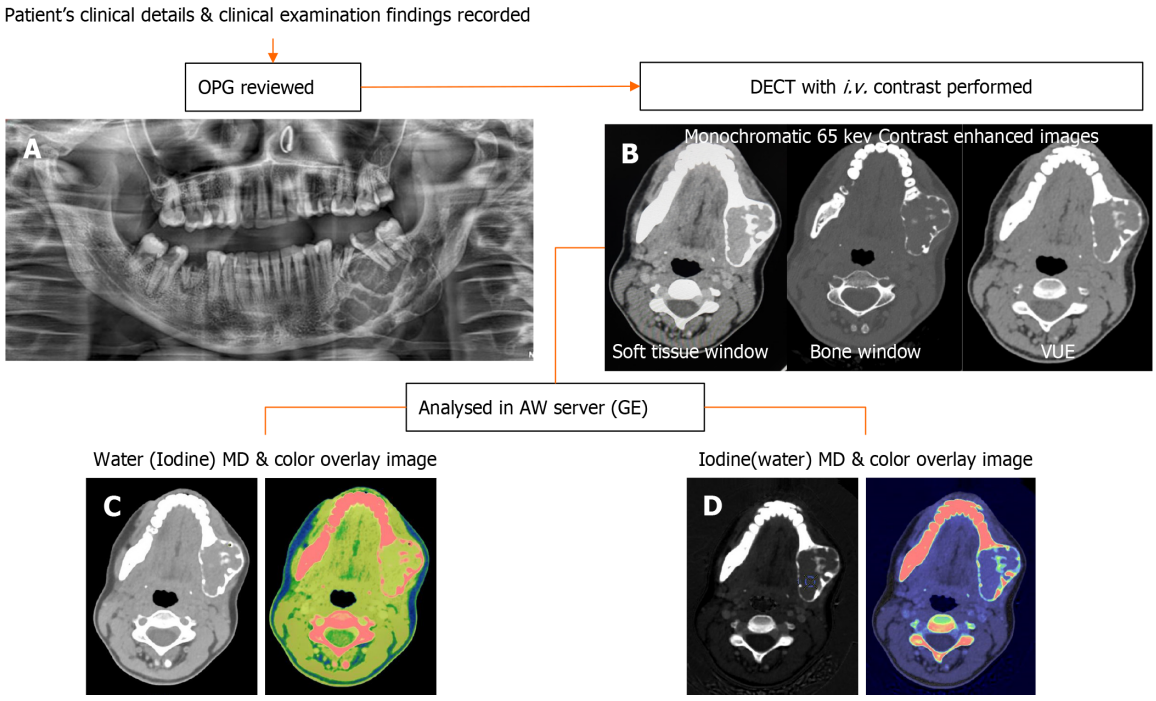

Figure 1 Workflow of patients undergoing dual-energy computed tomography Imaging. A: Orthopantomogram images are reviewed first; B: Followed by dual-energy computed tomography (DECT) acquisition using intravenous non-ionic iodinated contrast; C: Water (Iodine) with color overlay; D: Iodine (water) with color overlay are the material density images reconstructed in the dedicated software for quantitative analysis. DECT: Dual-energy computed tomography; OPG: Orthopantomography; MD: Material decomposition.

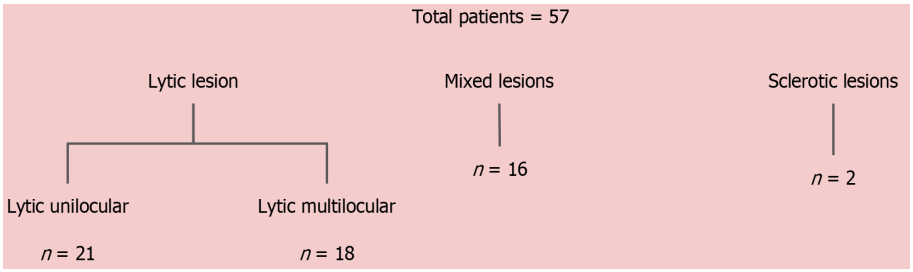

Figure 2 Classification of lesions based on computed tomography morphology (density and locularity).

RESULTS

Demographic and clinical characteristics

Fifty-seven patients (mean age, 37 ± 17 years, 26 males, and 31 females) were included in the study. The maximum number of patients was in the age group of 31-40 years (n = 14). The most common presenting complaint was swelling, which was seen in 96% of patients (n = 55), followed by local pain in 39% of patients (n = 22). The majority of the lesions (44%) were present for more than 6 months.

Histopathology results

In our study, histopathology was used as the gold standard for diagnosing jaw lesions. Twenty (35.09%) of the 57 patients had ameloblastomas, and 37 (64.91%) had non-ameloblastomas. With 11 cases, central giant cell granulomas (CGCG) were the most common lesions amongst non-ameloblastomas (29.7%). Table 1 summarizes the histopathological diagnosis of the lesions.

Morphological analysis on CECT

Of the 57 patients, 42 (73%) had lesions involving the mandible, and 13 (23%) had maxillary lesions, with thirteen patients having two lesions and two of them having three lesions. The morphological parameters were summarized for both ameloblastoma and non-ameloblastoma groups (Table 2). The ameloblastoma group showed a higher median volume (73.6 cm^3), more necrosis, a higher percentage of inferior alveolar canal involvement, retromolar trigone (RMT) involvement, and cortical involvement in the form of expansion or thinning. All these were statistically significant.

Table 1 Spectrum of lesions in histopathology

Final diagnosis	Number of lesions	Percentage (%)
Ameloblastomas	20	35
Central giant cell granuloma	11	19
Odontogenic keratocyst	6	10
Ossifying fibroma	5	8
Salivary gland tumors	2	4
Malignancy	3	5
Chondromyxoid fibroma	1	2
Non-tumorous	5	9
Sclerotic lesions	2	4
Ameloblastic fibroma	1	2
Odontogenic myxoma	1	2
Total	57	100

Table 2 Comparison of morphological characteristics between ameloblastoma and non-ameloblastoma groups

Variable	Ameloblastoma (*n* = 20)	Non-ameloblastoma (*n* = 37)	*P* value
Volume, cm^3	73.6 (7.6–1014)	39.12 (0.6–1296)	< 0.05
Cystic/necrotic areas	100	51	< 0.05
Cortical expansion/thinning	100	78	< 0.05
Mandibular canal involvement	60	32	< 0.05
Retromolar trigone involvement	45	18	< 0.05

Aggressive features evaluated in the case of mandibular tumors included mandibular canal involvement (*n* = 12), involvement of RMT (*n* = 16), condyle (*n* = 2), and coronoid process (*n* = 3). In cases of lesions in the maxilla, six cases showed aggressive features in the form of extension into the infratemporal fossa/orbit/pterygoid plates. Overall, locally aggressive features were seen in 19 cases (33%).

Quantitative analysis of solid components in contrast-enhanced DECT

On a broad comparison between the ameloblastoma and non-ameloblastoma groups, the ameloblastomas had a higher mean IC, a higher mean HU at 65 kev, a lower average NIC, and a lower WC compared to the non-ameloblastomas.

The ameloblastomas mostly had IC s in the 16–30 (moderate) mmol/mm^3 range and mean attenuation in the range of 50–150 HU. In contrast, 90% of CGCGs showed ICs greater than 31 mmol/mm^3 and mean attenuation > 150 HU. The OKCs had low values in all the parameters, distinctly different from others. The rest of them did not show any significant difference between them in their respective groups (Table 3). This could be attributed to the heterogeneous sample within the non-ameloblastoma group, which included cystic lesions with virtually no enhancing solid component and avidly enhancing masses. Statistical analysis revealed that the values of DECT parameters in OKCs and CGCCs were on the extreme opposite spectrum, with other lesions having values in between. Hence, we further subdivided the non-ameloblastoma group into three sub-groups and compared ameloblastomas with these three subgroups: OKCs, CGCG, and other jaw tumors.

Comparison between ameloblastoma and three major subgroups within the non-ameloblastoma group (Table 4):

When we compared ameloblastoma and central giant cell granuloma lesions (*n* = 31), significant differences were found in all quantitative DECT parameters ($P < 0.05$). CGCGs showed a higher average iodine content (36.1 × 100 *vs* 29.8 × 100 µg/cm^3), higher average WC (1042 × 1000 *vs* 1032 × 1000 mg/cm^3), a higher mean HU at 65 Kev (151 *vs* 122 HU), and a higher NIC (0.59 *vs* 0.34) compared to ameloblastomas (Figure 3).

In comparison between ameloblastomas and OKCs (*n* = 26), both groups showed significant differences in all the DECT parameters. However, the diagnostic dilemma lies in the distinction between UA and OKCs, which appear similar in morphology on conventional CT. Hence, to make this comparison impactful, we compared the WC of the cystic component in addition to the DECT parameters mentioned above between UA and OKCs. Interestingly, in addition to the above quantitative parameters, which were statistically significant, the WC of the cystic component also showed statistically significant differences between the two subgroups (Figure 4). In the OKCs, significantly higher water content within the cystic component was observed compared to ameloblastomas. When the ameloblastomas were compared with

Table 3 Classification of lesions based on iodine concentration (μg/mL)

Iodine concentration (μg/mL)	0-15 (low)	16-30 (moderate)	31-45 (high)	≥ 46 (extreme)
Ameloblastoma	2	11	4	1
CGCG	0	1	8	0
OKC	5	0	0	0
OF	0	3	0	0
Salivary gland tumor	1	1	0	0
Chondromyxoid fibroma	0	0	0	1
Others	4	6	2	1

All odontogenic keratocysts had a lower iodine concentration (0-15). Ameloblastomas predominantly had a moderate iodine concentration (16-30). Central giant cell granuloma predominantly had a higher iodine concentration (31-45). OKC: Odontogenic keratocysts; OF: Ossifying fibromas; CGCG: Central giant cell granuloma.

Table 4 Comparison of dual-energy computed tomography quantitative parameters between subgroups

Parameters	Amelo, mean ± SD	OKC, mean ± SD	CGCG, mean ± SD	Other JT, mean ± SD	[1]*P* value	[2]*P* value	[3]*P* value
Mean HU	122 ± 28.3	33 ± 12.4	151 ± 24.3	117 ± 37.9	0.007	< 0.001	0.616
IC	29 ± 9.3	7.2 ± 5.8	36.1 ± 6.8	24.8 ± 11.5	0.036	< 0.001	0.232
WC	1032.5 ± 13	1010 ± 11	1043 ± 11.6	1040 ± 11.4	0.036	0.044	0.056
NIC	0.35 ± 0.15	0.10 ± 0.1	0.59 ± 0.25	0.39 ± 0.24	0.011	0.007	0.501
WC (cystic)	997 ± 5.6	1020 ± 5	-	-	-	< 0.001	-

[1]*P* value obtained on comparison between ameloblastomas and central giant cell granulomas.
[2]*P* value obtained when unilocular ameloblastomas were compared with odontogenic keratocysts.
[3]*P* value obtained when ameloblastomas were compared with other jaw tumors.
Mean HU is the mean computed tomography density expressed in Hounsfield units. IC is the Iodine concentration of solid enhancing component expressed in 100 μg/cm^3. WC is the water concentration of solid enhancing component expressed in 1000 mg/cm^3. NIC is the normalized iodine concentration calculated as a ratio. WC (cystic) is the water concentration of cystic component calculated only in cases of unilocular ameloblastomas and OKCs. Other jaw tumor are a subgroup of lesions excluding ameloblastoma, CGCG and OKCs. IC: Iodine concentration; WC: Water concentration; NIC: Normalized iodine concentration; OKC: Odontogenic keratocyst; JT: Jaw tumor; CGCG: Central giant cell granuloma.

the "other jaw tumor" group, the former showed a higher average iodine content, although not statistically significant, and a lower WC, which was marginally significant compared to the latter (Figure 5).

Receiver operating characteristic analysis for calculating threshold values

The comparison of ameloblastomas and CGCG yielded statistically significant differences and satisfied the sample size for receiver operating characteristic (ROC) analysis. Hence, ROC analysis for all the DECT parameters was performed, and based on the AUC values, we selected a threshold for each parameter with the largest areas under the ROC curves (Table 5).

DECT evaluation of lesions based on morphology

Because the majority of jaw lesions are diagnosed using a systematic approach based on morphological appearance, we attempted to categorize the lesions based on density and locularity as described above and then studied their DECT parameters, except for the sclerotic lesions. The mean values of the DECT parameters of the lesions in the different morphological subgroups are summarized in Table 6.

DISCUSSION

We performed contrast-enhanced DECT with a predetermined split bolus contrast protocol in 57 patients with suspected maxillary and/or mandibular tumors or neoplasms after obtaining proper written informed consent, reviewing the clinical details, physical examination findings, and orthopantomogram. The morphological and quantitative spectral parameters obtained from DECT imaging were evaluated for the differentiation of various tumors of the jaw. The

Table 5 Receiver operating characteristic analysis of dual-energy computed tomography parameters between ameloblastoma and central giant cell granulomas

Variable	Cutoff value	Sensitivity, %	Specificity, %	AUC	SE
IC	32.1	81.82	65.00	0.727	0.0955
Mean HU	134	81.82	65.00	0.789	0.0832
WC	1036	72.73	50.00	0.6659	0.1
NIC	0.4	81.82	70.00	0.795	0.0970

Mean HU is the mean computed tomography density expressed in Hounsfield units. IC: Iodine concentration; WC: Water concentration; NIC: Normalized iodine concentration; AUC: The area under the receiver operating characteristic curve.

Table 6 Comparison of dual-energy computed tomography quantitative parameters based on morphology

Lytic unilocular (*n* = 21)	**Amelo, *n* = 7 (mean ± SD)**	**OKC, *n* = 6 (mean ± SD)**	**CGCG, *n* = 2 (mean ± SD)**	**OF, *n* = 2 (mean ± SD)**	**Non-tumorous, *n* = 4 (mean ± SD)**
Mean HU	115 ± 18.3	33 ± 12.4	135 ± 24	87 ± 17.9	67 ± 17.9
IC	28 ± 8.3	7.2 ± 5.8	32.9 ± 6.8	18.8 ± 9.5	8.8 ± 9.5
WC	1030.5 ± 12.8	1010 ± 11.3	1043 ± 11.6	1038 ± 11.4	1018 ± 11.4
NIC	0.37 ± 0.15	0.10 ± 0.1	0.72 ± 0.3	0.45 ± 0.24	0.25 ± 0.24
Lytic multilocular (*n* = 18)	**Amelo, *n* = 8 (mean ± SD)**	**CGCG, *n* = 4 (mean ± SD)**	**SG tumors, *n* = 2 (mean ± SD)**	**Malignancy, *n* = 3 (mean ± SD)**	**Non-tumorous, *n* = 1 (mean ± SD)**
Mean HU	123 ± 21.3	152 ± 20.4	94.2 ± 24.3	120 ± 37.9	69 ± 18.9
IC	29 ± 9.3	35.1 ± 9.8	17.85 ± 6.8	24.8 ± 11.5	10 ± 2.5
WC	1032.5 ± 12.8	1048 ± 11.3	1038 ± 11.6	1040 ± 11.4	1011 ± 11.4
NIC	0.35 ± 0.15	0.54 ± 0.19	0.18 ± 0.05	0.39 ± 0.24	0.29 ± 0.1
Mixed-sclerotic (*n* = 16)	**Amelo, *n* = 5 (mean ± SD)**	**CGCG, *n* = 5 (mean ± SD)**	**OFs, *n* = 4 (mean ± SD)**	**CMF, *n* = 1 (mean ± SD)**	**Non-tumorous, *n* = 1 (mean ± SD)**
Mean HU	129 ± 20.3	158 ± 20.4	143.8 ± 24.3	164 ± 37.9	77 ± 16
IC	29.5 ± 9.3	38.2 ± 9.8	31.1 ± 6.8	49.8 ± 11.5	11.8 ± 9
WC	1032.5 ± 12.8	1048 ± 11.3	1043 ± 11.6	1037 ± 11.4	1028 ± 20.4
NIC	0.35 ± 0.15	0.60 ± 0.19	0.66 ± 0.25	0.37 ± 0.24	0.19 ± 0.14

Amelo: Ameloblastoma; OKC: Odontogenic keratocysts; OF: Ossifying fibromas; CGCG: Central giant cell granuloma; SG tumors: Salivary gland tumors; IC: Iodine concentration; WC: Water concentration; NIC: Normalized iodine concentration; CMF: Chondromyxoid fibroma

primary goal of the study was to identify qualitative and quantitative parameters for distinguishing ameloblastomas from non-ameloblastomas.

There was a slight female predominance and the majority, *i.e.*, 77% of non-ameloblastomas comprised females compared to 35% in the ameloblastoma group. We studied the morphological features of lesions, and a comparison was made between the ameloblastoma and non-ameloblastoma groups. Median volume, degree of necrosis, inferior alveolar canal involvement, RMT involvement, and cortical involvement in the form of expansion or thinning were significantly higher in the ameloblastoma group. Our study agrees with these characteristics of ameloblastomas in other studies done previously in larger populations[7-10]. However, when the location was maxilla, there was no significant difference between the two groups. The rest of the variables, *i.e.*, margins, relation to teeth, and soft tissue extension, showed no statistically significant difference between the two groups.

In this study, we also investigated the potential of using quantitative information provided by both the virtual monochromatic images and MD images in dual-energy spectral CT imaging for the differentiation of ameloblastomas and non-ameloblastomas. Iodine, as the main component of a contrast medium, allows the assessment of vascular beds and intercellular spaces, and it facilitates the differentiation of lesions at various locations in the body based on the assumption that malignant, aggressive, or vascular lesions exhibit a higher degree of contrast enhancement[11]. DECT allows the quantitative assessment of the concentration of iodine accumulated in a unit of tissue volume. The degree of angiogenesis indicates the degree of viability, the degree of malignancy, and the vascularization sources[5,12]. Although there were no studies evaluating the role of DECT in jaw tumors, various studies done elsewhere in the head and region

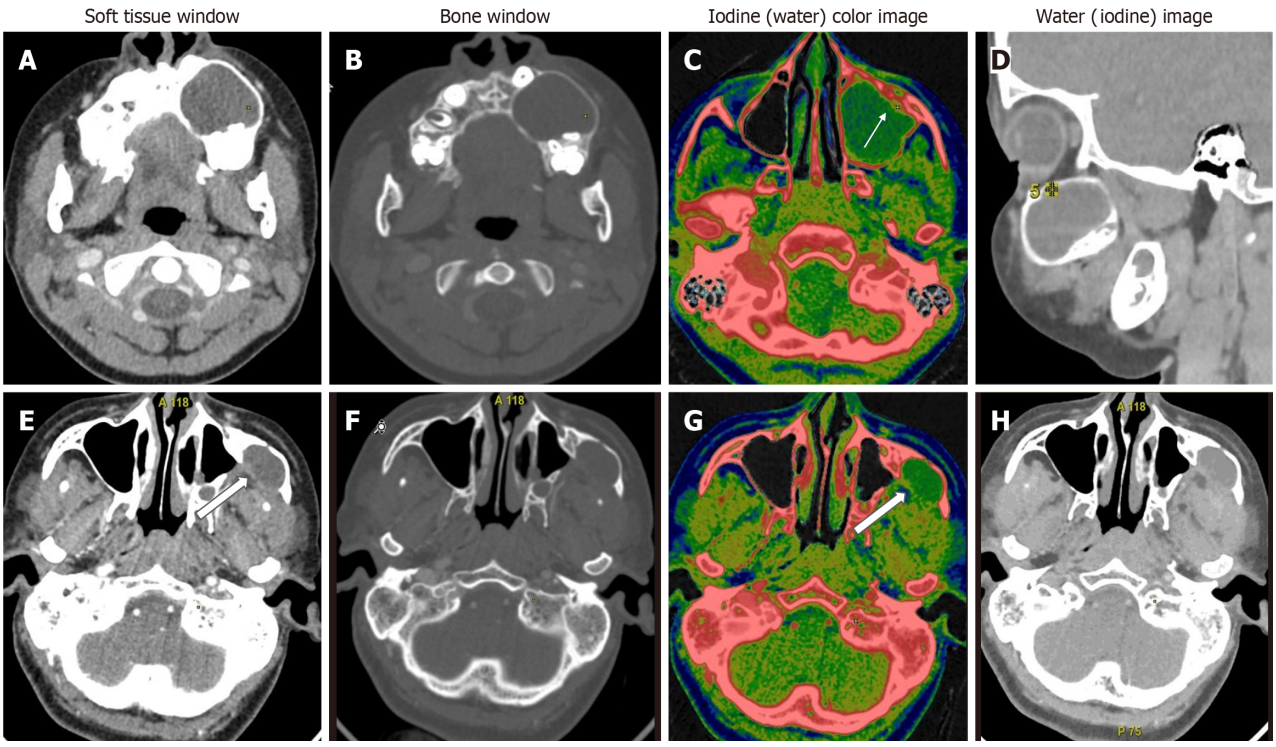

Figure 3 Unilocular lytic lesions differentiated based on water concentration. A-D: Unilocular ameloblastoma - contrast-enhanced dual-energy computed tomography images show a well-defined lytic unilocular cystic, expansile lesion in the left maxilla with mild peripheral rim enhancement better appreciated on iodine colour overlay images (white arrow). Water (iodine) material decomposition (MD) images showed a WC of 986 μg/cm^3 in the cystic component; E-H: Odontogenic keratocyst is also a well-defined lytic, unilocular cystic, expansile lesion in the left lateral wall of the maxillary sinus with a small enhancing mural component posteriorly (white open arrows). Water (Iodine) MD images revealed a water concentration of 1045 μg/cm^3 in the cystic component. In this case, due to the paucity of soft tissue components, iodine concentration did not help; however, the water concentration of the cystic component differed significantly, aiding in the diagnosis.

showed MD images, especially IC images, can be used for the differentiation of various pathologies[4]. This was because it is now known that the IC value is more accurate than the CT value in assessing the blood supply to a lesion.

The higher IC in ameloblastomas can be attributed to the fact that these are slow-growing, locally invasive tumors with an explicit biologic pattern. Multiple stromal factors, including growth and angiogenic factors, extracellular matrix components, and proteinases, are overexpressed and linked to the development of this tumor, where they play critical roles in invasion, growth, and progression with aggressive behavior. This could explain the rise in metabolic activity in ameloblastoma connective tissue[13-16]. The non-ameloblastomas included a heterogeneous sample within the group that ranged from cystic lesions with enhancing wall/septae and virtually no enhancing mural component like OKCs to avidly enhancing solid lesions like CGCGs. This was also supported by the fact that statistical analysis revealed that the values of DECT parameters in OKCs and CGCCs were on the extreme opposite spectrum, with other lesions having values ranging in between. This led to further classification of the non-ameloblastomas and their comparison with ameloblastomas.

On the first comparison between ameloblastomas and CGCG, the CGCGs had higher mean iodine, water, mean HU at 65 Kev, and NIC compared to ameloblastomas. This was in accordance with the earlier studies, which showed that central giant cell lesions had significantly higher angiogenetic potential compared to ameloblastomas[17,18]. The differential analysis based on the calculated threshold IC value showed that a value of 32.1 × 100 μg/cm^3, best represented the differences based on the AUC values on the ROC curves, with a sensitivity and specificity of 81.8% and 65%, respectively.

In a comparison of ameloblastomas with OKCs, similar to morphological features, all quantitative parameters showed significant differences between the two lesions in our study[19]. Interestingly, in addition to the DECT quantitative parameters of enhancing components, the WC of the cystic component also showed a statistically significant difference between the two subgroups. In the OKCs, significantly higher water content within the cystic component was observed compared to ameloblastomas (1020 *vs* 997 μg/cm^3). Our study showed that UA and OKCs could be effectively differentiated on the basis of the IC and WC measurements of the cystic component, as these lesions are often purely cystic (Figure 4). Our finding that the WC of the cystic areas differs significantly between the ameloblastomas and OKCs indicates that the density of the cystic components with suppressed iodine information varies between these odontogenic tumors. Cystic spaces in the ameloblastomas usually contain slightly proteinaceous fluids, occasionally associated with colloidal materials[20]. The cyst lumen of OKCs often contains desquamated keratin. This desquamated keratin accumulates in such large quantities that it influences the attenuations on CT images, which was even proven in an experimental study by Yoshiura *et al*[21]. Therefore, it is plausible that such desquamated keratin increased the viscosity of fluids in the lumen, thereby increasing the value of WC in the water (iodine) images compared with ameloblastomas, in which increases in viscosity may be minimal.

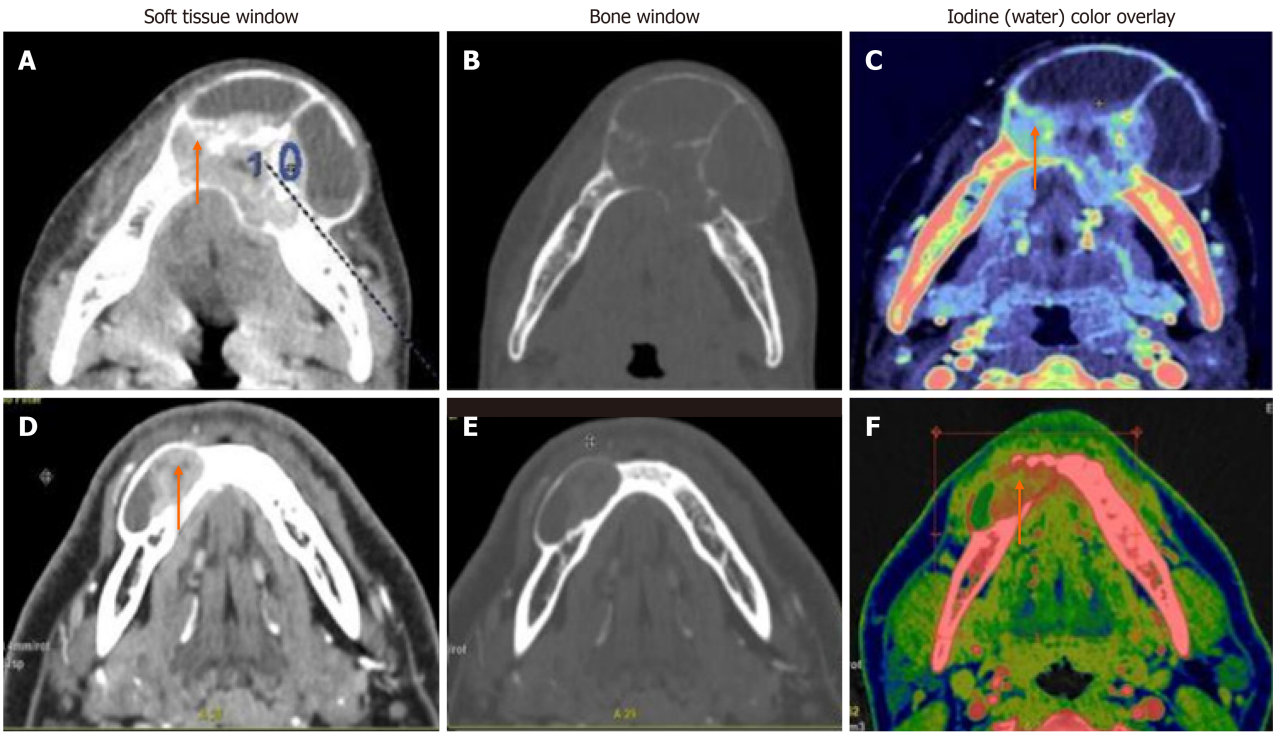

Figure 4 Multilocular solid-cystic lesions differentiated based on iodine concentration. A-C: Central giant cell granuloma - A well-defined expansile multiloculated solid-cystic tumor in the left anterior mandible crossing the midline. Iodine images with a color overlay (C) showed an iodine concentration (IC) of 57 × 100 μg/cm^3 of the solid enhancing part (orange arrow); D-F: Ameloblastoma - a well-defined lytic, unilocular, solid-cystic, expansile lesion with an enhancing soft tissue component (orange arrow). Iodine images with a color overlay (F) show increased iodine content (areas in red) within the soft tissue (IC of 23 × 100 μg/cm^3).

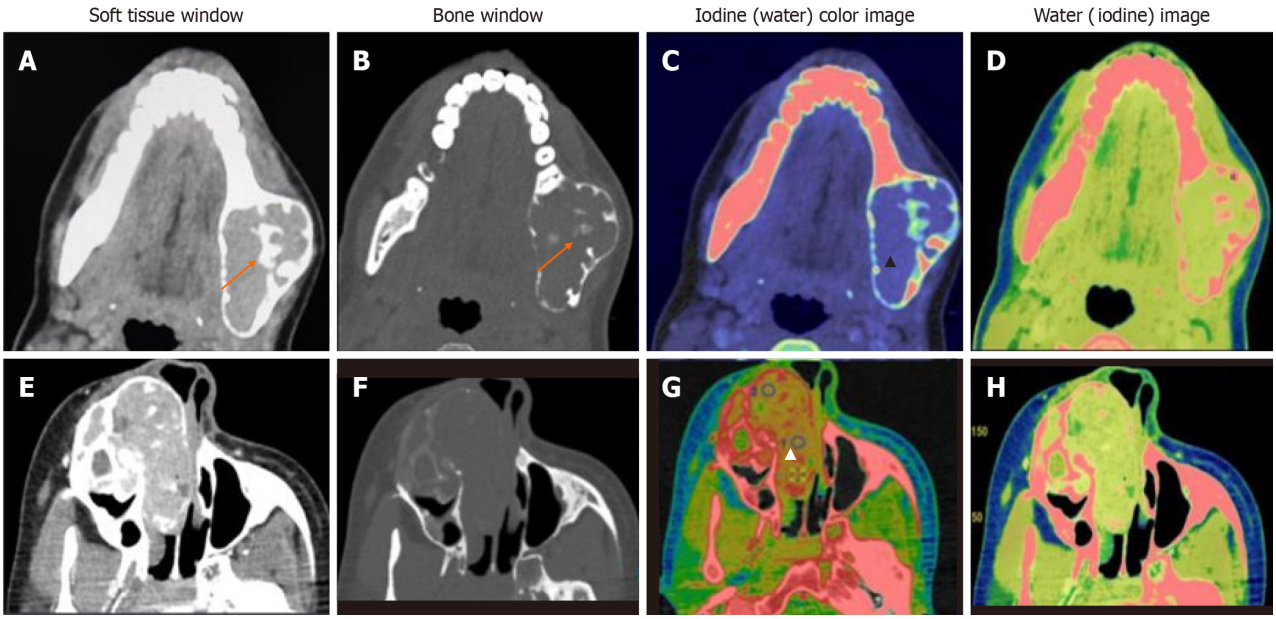

Figure 5 Mixed lytic-sclerotic lesions. A-D: Central giant cell granuloma well-defined, mixed lytic-sclerotic buccolingual expansile lesion with a narrow zone of transition. Central ossific foci are seen (orange arrows). Iodine (water) material decomposition overlay images show a mild, homogeneous iodine concentration (blue region within the tumor - black arrowhead) (C). Water (Iodine) images show no cystic or necrotic areas (D); E-H: Ossifying fibroma well- defined expansile mass epicentered in the right maxilla, showing heterogeneous enhancement in its lytic soft tissue component with multiple sclerotic foci extending into the nasal cavity (E). The iodine image shows foci of increased iodine concentration (red areas - white arrowhead) (G). Lower iodine concentration and higher water concentration were seen in the latter, which suggested “other jaw tumor” as in this case.

The above comparisons yielded an interesting fact: Ameloblastomas showed significantly increased values of DECT parameters, which were indirect markers of vascularity, compared to non-ameloblastomas except for the CGCG. As we can see, the latter has a significantly increased IC, mean HU value, WC, and NIC compared to ameloblastomas. The flowchart (Figure 6) presents an algorithmic approach to classifying jaw lesions based on differences in DECT quantitative parameters in our study.

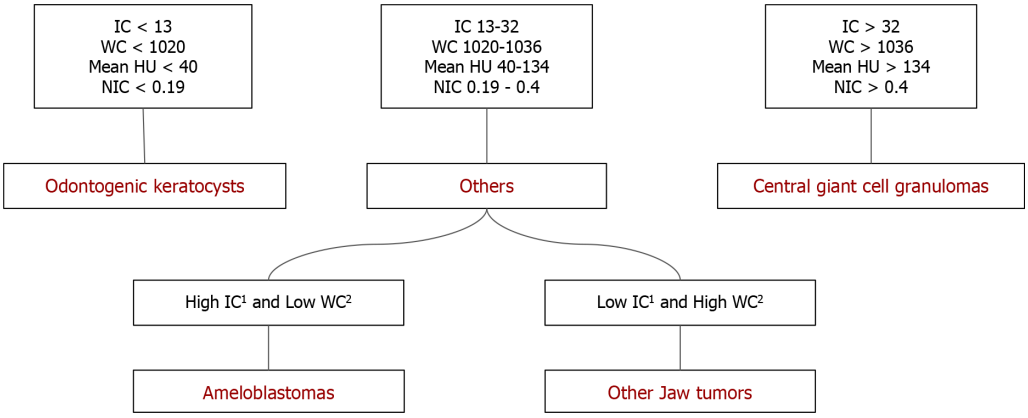

Figure 6 Flowchart showing algorithmic differentiation of jaw tumors in the study population based on the quantitative analysis. Central giant cell granulomas had higher iodine concentration (IC), water concentration (WC), and normalized IC (NIC), odontogenic keratocysts with lower IC, WC, and NIC, ameloblastomas and other jaw tumor group showed values in between. Between the two, ameloblastomas had higher IC with lower WC while other jaw tumor group had lower IC with higher WC. [1]Not significant; [2]Marginally significant. WC: Water concentration; IC: Iodine concentration; NIC: Normalized iodine concentration.

The major limitation of the present study was the heterogeneous sample within the "other jaw tumor" group, which resulted in a limited comparison of separate pathological lesions. Another limitation was the inability to compare the DECT parameters based on the morphological subgroups due to the limited sample size.

CONCLUSION

We propose that DECT can help with both morphological and functional classification of jaw tumors, as well as distinguish between various jaw tumors that closely resemble each other in conventional imaging. Our study contributes to the existing body of literature, confirming the technical feasibility of single-source spectral CT imaging, which relies on the differentiation of iodine and water, as a valuable tool for quantitatively distinguishing ameloblastoma from other jaw tumors at about comparable dose equivalency of traditional CT. Additionally, our research marks the pioneering use of DECT in characterizing and differentiating various jaw tumors.

ACKNOWLEDGEMENTS

Faculty, residents, and radiographers of the Department of Radiodiagnosis and Interventional Radiology, All India Institute of Medical Sciences, New Delhi for their support and assistance. Mr. Hem Sati, Department of Biostatistics, AIIMS, New Delhi, for biostatistical guidance.

FOOTNOTES

Author contributions: Viswanathan DJ, Bhalla AS and Manchanda S designed the research study; Viswanathan DJ performed the research; Roychoudhury A contributed to referral of cases and surgical input; Mishra D and Mriddha AR contributed to histopathological analysis and pathological insight; Viswanathan DJ analyzed the data and wrote the manuscript; All authors have read and approved the final manuscript.

Institutional review board statement: The study was reviewed and approved by the All India Institute of Medical Sciences, New Delhi Institutional Review Board (No. IECPG-354/22.07.2020, RT-2/26.08.2020).

Informed consent statement: All patients give their full informed consent.

Conflict-of-interest statement: All the authors report no relevant conflicts of interest for this article.

Data sharing statement: Technical appendix, statistical code, and dataset available from the corresponding author at ashubhalla2@gmail.

com. Participants gave informed consent for data sharing.

STROBE statement: The authors have read the STROBE Statement—checklist of items, and the manuscript was prepared and revised according to the STROBE Statement—checklist of items.

Country/Territory of origin: India

ORCID number: Deepak Justine Viswanathan 0000-0001-8169-6115; Ashu Seith Bhalla 0000-0003-2200-2544.

S-Editor: Li L
L-Editor: A
P-Editor: Zhao S

REFERENCES

1 **Soluk-Tekkeşin M**, Wright JM. The World Health Organization Classification of Odontogenic Lesions: A Summary of the Changes of the 2017 (4th) Edition. *Turk Patoloji Derg* 2018; **34** [PMID: 28984343 DOI: 10.5146/tjpath.2017.01410]
2 **Dunfee BL**, Sakai O, Pistey R, Gohel A. Radiologic and pathologic characteristics of benign and malignant lesions of the mandible. *Radiographics* 2006; **26**: 1751-1768 [PMID: 17102048 DOI: 10.1148/rg.266055189]
3 **McCollough CH**, Leng S, Yu L, Fletcher JG. Dual- and Multi-Energy CT: Principles, Technical Approaches, and Clinical Applications. *Radiology* 2015; **276**: 637-653 [PMID: 26302388 DOI: 10.1148/radiol.2015142631]
4 **Roele ED**, Timmer VCML, Vaassen LAA, van Kroonenburgh AMJL, Postma AA. Dual-Energy CT in Head and Neck Imaging. *Curr Radiol Rep* 2017; **5**: 19 [PMID: 28435761 DOI: 10.1007/s40134-017-0213-0]
5 **Tawfik AM**, Razek AA, Kerl JM, Nour-Eldin NE, Bauer R, Vogl TJ. Comparison of dual-energy CT-derived iodine content and iodine overlay of normal, inflammatory and metastatic squamous cell carcinoma cervical lymph nodes. *Eur Radiol* 2014; **24**: 574-580 [PMID: 24081649 DOI: 10.1007/s00330-013-3035-3]
6 **Luo S**, Sha Y, Wu J, Lin N, Pan Y, Zhang F, Huang W. Differentiation of malignant from benign orbital tumours using dual-energy CT. *Clin Radiol* 2022; **77**: 307-313 [PMID: 35094818 DOI: 10.1016/j.crad.2021.12.019]
7 **MacDonald-Jankowski DS**, Yeung R, Lee KM, Li TK. Odontogenic myxomas in the Hong Kong Chinese: clinico-radiological presentation and systematic review. *Dentomaxillofac Radiol* 2002; **31**: 71-83 [PMID: 12076060 DOI: 10.1038/sj.dmfr.4600678]
8 **Wu PC**, Chan KW. A survey of tumours of the jawbones in Hong Kong Chinese: 1963-1982. *Br J Oral Maxillofac Surg* 1985; **23**: 92-102 [PMID: 3158339 DOI: 10.1016/0266-4356(85)90058-0]
9 **Reichart PA**, Philipsen HP, Sonner S. Ameloblastoma: biological profile of 3677 cases. *Eur J Cancer B Oral Oncol* 1995; **31B**: 86-99 [PMID: 7633291 DOI: 10.1016/0964-1955(94)00037-5]
10 **Siar CH**, Lau SH, Ng KH. Ameloblastoma of the jaws: a retrospective analysis of 340 cases in a Malaysian population. *J Oral Maxillofac Surg* 2012; **70**: 608-615 [PMID: 21723654 DOI: 10.1016/j.joms.2011.02.039]
11 **Sanghavi PS**, Jankharia BG. Applications of dual energy CT in clinical practice: A pictorial essay. *Indian J Radiol Imaging* 2019; **29**: 289-298 [PMID: 31741598 DOI: 10.4103/ijri.IJRI_241_19]
12 **Li L**, Zhao Y, Luo D, Yang L, Hu L, Zhao X, Wang Y, Liu W. Diagnostic value of single-source dual-energy spectral computed tomography in differentiating parotid gland tumors: initial results. *Quant Imaging Med Surg* 2018; **8**: 588-596 [PMID: 30140621 DOI: 10.21037/qims.2018.07.07]
13 **Chi AC**, Neville BW. Odontogenic Cysts and Tumors. *Surg Pathol Clin* 2011; **4**: 1027-1091 [PMID: 26837786 DOI: 10.1016/j.path.2011.07.003]
14 **Ribeiro BF**, Iglesias DP, Nascimento GJ, Galvão HC, Medeiros AM, Freitas RA. Immunoexpression of MMPs-1, -2, and -9 in ameloblastoma and odontogenic adenomatoid tumor. *Oral Dis* 2009; **15**: 472-477 [PMID: 19522745 DOI: 10.1111/j.1601-0825.2009.01575.x]
15 **Wang A**, Zhang B, Huang H, Zhang L, Zeng D, Tao Q, Wang J, Pan C. Suppression of local invasion of ameloblastoma by inhibition of matrix metalloproteinase-2 in vitro. *BMC Cancer* 2008; **8**: 182 [PMID: 18588710 DOI: 10.1186/1471-2407-8-182]
16 **Jamshidi S**, Zargaran M, Baghaei F, Shojaei S, Zare Mahmoodabadi R, Dehghan A, Moghimbeigi A. An Immunohistochemical Survey to Evaluate the Expression of CD105 and CD34 in Ameloblastoma and Odontogenic Keratocyst. *J Dent (Shiraz)* 2014; **15**: 192-198 [PMID: 25469359]
17 **Ali K**, Zeb Khan S, Sultana N, Alghamdi O, Muhammad S, Mokeem SA, Ali S, Abduljabbar T, Vohra F. Assessment of Tumor Angiogenesis by Expression of CD 105 in Ameloblastoma, Odontogenic Keratocyst and Central Giant Cell Lesion. *Asian Pac J Cancer Prev* 2020; **21**: 3373-3379 [PMID: 33247698 DOI: 10.31557/APJCP.2020.21.11.3373]
18 **Ghosh A**, Lakshmanan M, Manchanda S, Bhalla AS, Kumar P, Bhutia O, Mridha AR. Contrast-enhanced multidetector computed tomography features and histogram analysis can differentiate ameloblastomas from central giant cell granulomas. *World J Radiol* 2022; **14**: 329-341 [PMID: 36186516 DOI: 10.4329/wjr.v14.i9.329]
19 **Hayashi K**, Tozaki M, Sugisaki M, Yoshida N, Fukuda K, Tanabe H. Dynamic multislice helical CT of ameloblastoma and odontogenic keratocyst: correlation between contrast enhancement and angiogenesis. *J Comput Assist Tomogr* 2002; **26**: 922-926 [PMID: 12488736 DOI: 10.1097/00004728-200211000-00011]
20 **Smoker WR**, Harnsberger HR. Differential diagnosis of head and neck lesions based on their space of origin. 2. The infrahyoid portion of the neck. *AJR Am J Roentgenol* 1991; **157**: 155-159 [PMID: 2048511 DOI: 10.2214/ajr.157.1.2048511]

21 **Yoshiura K**, Higuchi Y, Ariji Y, Shinohara M, Yuasa K, Nakayama E, Ban S, Kanda S. Increased attenuation in odontogenic keratocysts with computed tomography: a new finding. *Dentomaxillofac Radiol* 1994; **23**: 138-142 [PMID: 7530666 DOI: 10.1259/dmfr.23.3.7530666]

World Journal of Radiology

Submit a Manuscript: https://www.f6publishing.com

World J Radiol 2024 April 28; 16(4): 94-108

DOI: 10.4329/wjr.v16.i4.94

ISSN 1949-8470 (online)

ORIGINAL ARTICLE

Observational Study

Pseudoaneurysm formation following transarterial embolization of traumatic carotid-cavernous fistula with detachable balloon: An institutional cohort long-term study

Prasert Iampreechakul, Korrapakc Wangtanaphat, Songpol Chuntaroj, Yodkhwan Wattanasen, Sunisa Hangsapruek, Punjama Lertbutsayanukul, Pimchanok Puthkhao, Somkiet Siriwimonmas

Specialty type: Radiology, nuclear medicine and medical imaging

Provenance and peer review: Invited article; Externally peer reviewed.

Peer-review model: Single blind

Peer-review report's classification

Scientific Quality: Grade D
Novelty: Grade C
Creativity or Innovation: Grade B
Scientific Significance: Grade C

P-Reviewer: Lei T, China

Received: December 11, 2023
Revised: April 4, 2024
Accepted: April 16, 2024
Published online: April 28, 2024

Prasert Iampreechakul, Korrapakc Wangtanaphat, Department of Neurosurgery, Neurological Institute of Thailand, Bangkok 10400, Thailand

Songpol Chuntaroj, Yodkhwan Wattanasen, Sunisa Hangsapruek, Punjama Lertbutsayanukul, Department of Neuroradiology, Neurological Institute of Thailand, Bangkok 10400, Thailand

Pimchanok Puthkhao, Department of Medical Services, Neurological Institute of Thailand, Bangkok 10400, Thailand

Somkiet Siriwimonmas, Department of Radiology, Bumrungrad International Hospital, Bangkok 10110, Thailand

Corresponding author: Prasert Iampreechakul, MD, Staff Physician, Department of Neurosurgery, Neurological Institute of Thailand, Ratchawithi Road, Khwaeng Thung Phaya Thai, Bangkok 10400, Thailand. bangruad@hotmail.com

Abstract

BACKGROUND

The goal of therapy for traumatic carotid-cavernous fistula (TCCF) is the elimination of fistula while maintaining patency of the parent artery. The treatment for TCCF has evolved from surgery to endovascular management using detachable balloons, coils, liquid embolic agents, covered stents, or flow-diverter stent through arterial or venous approaches. Despite the withdrawal of detachable balloons from the market in the United States since 2004, transarterial embolization with detachable balloons has currently remained the best initial treatment for TCCF in several countries. However, the pseudoaneurysm formation following transarterial detachable balloon embolization has rarely been observed in long-term follow-up.

AIM

To determine the occurrence and long-term follow-up of pseudoaneurysm after transarterial detachable balloon for TCCF.

METHODS

Between January 2009 and December 2019, 79 patients diagnosed with TCCF were

treated using detachable latex balloons (GOLDBAL) of four sizes. Pseudoaneurysm sizes were stratified into five grades for analysis. Initial and follow-up assessments involved computed tomography angiography at 1 month, 6 month, 1 year, and longer intervals for significant cases. Clinical follow-ups occurred semi-annually for 2 years, then annually. Factors analyzed included sex, age, fistula size and location, and balloon size.

RESULTS

In our cohort of 79 patients treated for TCCF, pseudoaneurysms formed in 67.1%, with classifications ranging from grade 0 to grade 3; no grade 4 or giant pseudoaneurysms were observed. The majority of pseudoaneurysms did not progress in size, and some regressed spontaneously. Calcifications developed in most large pseudoaneurysms over 5-10 years. Parent artery occlusion occurred in 7.6% and recurrent fistulas in 16.5%. The primary risk factors for pseudoaneurysm formation were identified as the use of specific balloon sizes, with balloon SP and No. 6 significantly associated with its occurrence (P = 0.005 and P = 0.002, respectively), whereas sex, age, fistula size, location, and the number of balloons used were not significant predictors.

CONCLUSION

Pseudoaneurysm formation following detachable balloon embolization for TCCF is common, primarily influenced by the size of the balloon used. Despite this, all patients with pseudoaneurysms remained asymptomatic during long-term follow-up.

Key Words: Pseudoaneurysm formation; Traumatic carotid-cavernous fistula; Direct carotid-cavernous fistula; Transarterial embolization; Detachable balloon; Endovascular treatment; Computed tomography angiography; Long-term follow-up

Core Tip: This study investigated the incidence and determinants of pseudoaneurysm formation following transarterial detachable balloon embolization in treating traumatic carotid-cavernous fistula over a decade. It highlighted balloon size as a significant risk factor, with larger balloons notably increasing pseudoaneurysm occurrence. Despite the high incidence of pseudoaneurysms, all affected patients remained asymptomatic through long-term follow-up, underscoring the procedure's overall safety. These findings emphasize the critical role of selecting appropriate balloon sizes to mitigate risk and optimize outcomes, offering valuable insights for clinicians in managing this complex condition effectively.

Citation: Iampreechakul P, Wangtanaphat K, Chuntaroj S, Wattanasen Y, Hangsapruek S, Lertbutsayanukul P, Puthkhao P, Siriwimonmas S. Pseudoaneurysm formation following transarterial embolization of traumatic carotid-cavernous fistula with detachable balloon: An institutional cohort long-term study. *World J Radiol* 2024; 16(4): 94-108
URL: https://www.wjgnet.com/1949-8470/full/v16/i4/94.htm
DOI: https://dx.doi.org/10.4329/wjr.v16.i4.94

INTRODUCTION

Traumatic carotid-cavernous fistulas (TCCFs) are high-flow shunts directly communicated between the cavernous segment of the internal carotid artery (ICA) and the cavernous sinus, resulting from trauma[1]. TCCFs were categorized as Type A by the Barrow classification of CCFs[2]. Spontaneous resolution of TCCFs is extremely rare[3]. The typical clinical manifestations, which depend on the venous drainage of the cavernous sinus, include pulsatile proptosis, conjunctival chemosis, red eye, and/or audible bruit. Rarely, aggressive neurological symptoms, especially deterioration of consciousness, may develop due to cortical venous reflux, leading to cerebral ischemia and/or hemorrhage[4].

The management of TCCFs has evolved significantly, transitioning from surgical to endovascular methods, utilizing detachable balloons or coils through arterial or venous approaches[5]. The first case of endovascular occlusion of TCCF using a fixed balloon catheter was described by Prolo and Hanberry[6] in 1971. Later, Serbinenko[7], a Russian neurosurgeon, pioneered the use of detachable balloons for TCCF treatment while preserving the ICA in 1974. This technique led to a new era for management of TCCF by the endovascular route. Subsequently, Debrun *et al*[8-10] developed another version of detachable balloon, and transarterial detachable balloon embolization became more popularized for treatment of TCCF in many countries for many years. However, there were some balloon-related complications including premature deflation, early detachment, and/or balloon migration resulting in recurrence of the fistula, ischemic stroke, or pseudoaneurysm formation[11-17]. In 2004, detachable balloons were withdrawn from the market in the United States, and detachable coils were used instead for occlusion of TCCF[18]. Nevertheless, detachable balloon embolization currently remains the preferred treatment option for TCCF in several countries including ours[5,19-21].

The pseudoaneurysm formation following endovascular treatment of TCCF with detachable balloon has rarely been observed, especially in long-term follow-up[12,22]. We conducted a retrospective cohort study to ascertain the occurrence and long-term follow-up of pseudoaneurysm after transarterial embolization of TCCF with detachable balloons. Risk

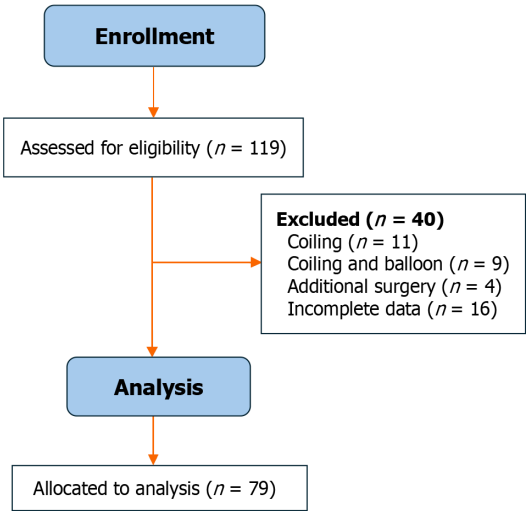

Figure 1 Flow chart of the study.

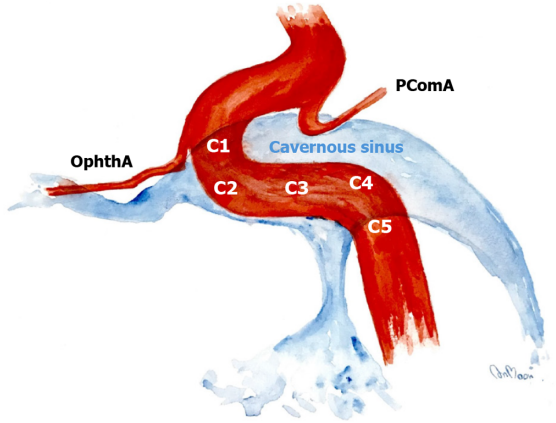

Figure 2 Location of the fistula. Schematic diagram illustrating the segments of the cavernous internal carotid artery, which is divided into five segments including: C1, anterior ascending segment; C2, junction between the anterior ascending and horizontal segment; C3, horizontal segment; C4, junction between the horizontal and posterior ascending segment; and C5, posterior ascending segment. OphthA: Ophthalmic artery; PComA: Posterior communicating artery.

factors for the occurrence of pseudoaneurysm were also investigated.

MATERIALS AND METHODS

Study population and data collection

This retrospective cohort study was conducted at a tertiary neurosurgical center, with ethics committee approval from our institute. From January 2009 to December 2019, 119 consecutive patients with TCCF were recruited. Inclusion criteria were patients with TCCF treated by transarterial embolization using detachable balloons. The exclusion criteria were patients with TCCF treated by other options, including coiling (n = 11), coiling and balloon (n = 9), and combined endovascular and surgical treatment (n = 4). In addition, 16 patients with incomplete data were excluded from enrollment. The final cohort of our study included 79 patients (56 males and 71 females). Their age ranged from 11 years to 68 years, with a mean age of 34.82 ± 13.01 years. The flow chart of our study is illustrated in Figure 1.

Diagnosis was based on symptoms, trauma history, medical examination, computed tomography (CT) scan, and cerebral angiography. Demographic data collected included age, sex, cause of injury, and clinical symptoms at presentation.

Study assessment and criteria

The fistula location was classified into five regions according to the cavernous ICA segmentation as described by Debrun *et al*[12]. These segments of ICA included C1 (anterior ascending segment), C2 (junction between the anterior ascending and horizontal segment), C3 (horizontal segment), C4 (junction between the horizontal and posterior ascending segment), and C5 (posterior ascending segment; Figure 2).

Table 1 Commonly used detachable balloons in the present study

Balloon size	Maximum volume in mL	Inflated dimensions in mm, diameter × length
GOLDBAL 4	0.75	9 × 16
GOLDBAL 5	2.50	12 × 28
GOLDBAL 6	3.00	15 × 25
GOLDBAL SP	0.90	12 × 13

Based on the study of Chi *et al*[20], we classified the size of the fistula as small, medium, and large. Small-sized fistulas had good antegrade ipsilateral ICA flow, represented by opacification of both the anterior cerebral artery (ACA) and middle cerebral artery (MCA). Medium-sized fistulas had fair antegrade flow, represented by opacification of either the ACA or MCA. Large-sized fistulas had poor antegrade flow, represented by opacification of neither the ACA nor MCA (Figure 3).

The size of pseudoaneurysms was stratified by five grades including: Grade 0, no pseudoaneurysm; grade 1, small pseudoaneurysm (< 5 mm); grade 2, medium (5–10 mm); grade 3, large (11–25 mm); and grade 4, giant (> 25 mm).

The detachable latex balloon (GOLDBAL; Balt Extrusion, Montmorency, France) with four different sizes, including balloon No. 4, No. 5, No 6., and SP, was used in our study (Table 1). SP is abbreviated from the name and surname of Professor Sirintara Pongpech, Thai neurointerventionist, who designed this balloon size. Balloon SP contains a maximum volume of 0.9 mL and expands to 12 mm × 13 mm.

Following transarterial balloon embolization, all patients underwent CT angiography (CTA) at 1 mo. If pseudoaneurysms occurred, CTA follow-up was performed at 6 month and 1 year. For large-sized pseudoaneurysm (grade 3) or giant (grade 4) pseudoaneurysm, CTA follow-up was carried out every 1 year to 3 years. The clinical follow-up was conducted every 3 month to 6 month for 2 years after the procedure and annually thereafter. Factors including sex, age, size and location of fistula, number of balloons, and the size of balloon, were statistically analyzed. All images were evaluated independently by the experienced neuroradiologist (SH) using Picture Archiving and Communication System (PACS; FUJIFILM, Stamford, CT, United States).

Neurointerventional techniques

All endovascular procedures were performed under general anesthesia in a specialized biplane neuroangiography suite. Using the transfemoral approach, a 9 F introducing catheter was positioned into the cervical ICA. Subsequently, cerebral angiography was performed to assess the location and size of fistula, presence of any collateral supply through the circle of Willis, and venous drainage pattern. Additionally, contralateral carotid angiography during compression of the ipsilateral carotid artery was carried out to evaluate function of the anterior communicating artery. The precise fistula site was delineated by vertebral artery injection with simultaneous ipsilateral carotid compression. Following systemic heparinization, the balloon mouthed delivery microcatheter (Baltacci; Balt, Montmorency, France) was cautiously navigated by flow guidance into the orifice of the fistula under fluoroscopic road-mapping (Figures 4 and 5). The balloon was gradually inflated with iodinated contrast media, ensuring it did not exceed the maximum volume specified by the manufacturer for each balloon size (Table 1). Following the obliteration of the fistula by confirmation through a contrast media injection *via* the guiding catheter, the balloon was detached by gently pulling the microcatheter. Immediate post-embolization angiography was then performed to verify complete closure of the fistula. Multiple detachable balloons might be required if a single balloon failed to completely occlude TCCF. Post-procedure, all patients were advised absolute bed rest for 72 h to prevent balloon migration.

Statistical analysis

Data analysis was performed using the SPSS 16.0 software package (SPSS Inc, Chicago, IL, United States). Continuous data were expressed as mean (standard deviation) or median (interquartile range), and categorical variables were presented as numbers and corresponding percentages. Differences between groups were assessed using the Kruskal-Wallis test for continuous variables and Pearson Chi-square or Fisher's exact tests for categorical variables. A P value < 0.05 was considered statistically significant.

RESULTS

Study population and demographics

Patient and fistula characteristics are summarized in Table 2. The causes of injury were predominantly motor vehicle accidents (75 patients, 94.9%), followed by assault (2 patients, 2.5%), falling from height (1 patient, 1.27%), and gunshot injury (1 patient, 1.27%). Clinical manifestations included pulsating proptosis (61 patients, 77.2%), conjunctival chemosis (39 patients, 49.4%), red eye (49 patients, 62.0%), audible bruit (28 patients, 35.4%), cranial nerve palsy (8 patients, 10.1%), and hemiparesis (2 patients, 2.5%).

Table 2 Summary of the 79 patients treated with transarterial balloon embolization

Patient characteristics	Number of patients, *n* (%)
Sex	
Male	56 (70.9)
Female	23 (29.1)
Cause of injury	
Motor vehicle accident	75 (94.9)
Assault	2 (2.5)
Falling from height	1 (1.27)
Gunshot wound	1 (1.27)
Symptoms	
Pulsatile proptosis	61 (77.2)
Conjunctival chemosis	39 (49.4)
Red eye	49 (62.0)
Tinnitus	28 (35.4)
Visual impairment	9 (11.4)
Cranial nerve palsy	8 (10.1)
Hemiparesis	2 (2.5)
Fistula characteristics	
Side	
Right	40 (50.6)
Left	39 (49.4)
Location	
C1	1 (1.3)
C2	7 (8.9)
C3	26 (32.9)
C4	25 (31.6)
C5	20 (25.3)
Size	
Small	14 (17.7)
Medium	31 (39.2)
Large	34 (43.1)
Result of treatment	
Number of balloons used	
One	51(64.6)
Two	20 (25.3)
Three	8 (10.1)
Recurrence of fistula	13 (16.5)
ICA preservation	73 (92.4)
The occurrence of pseudoaneurysm	
Grade 0-No pseudoaneurysm	24 (32.9)
Grade 1-Small pseudoaneurysm	22 (30.1)
Grade 2-Medium pseudoaneurysm	18 (24.7)

Grade 3-Large pseudoaneurysm	9 (12.3)
Grade 4-Giant pseudoaneurysm	0 (0)

ICA: Internal carotid artery.

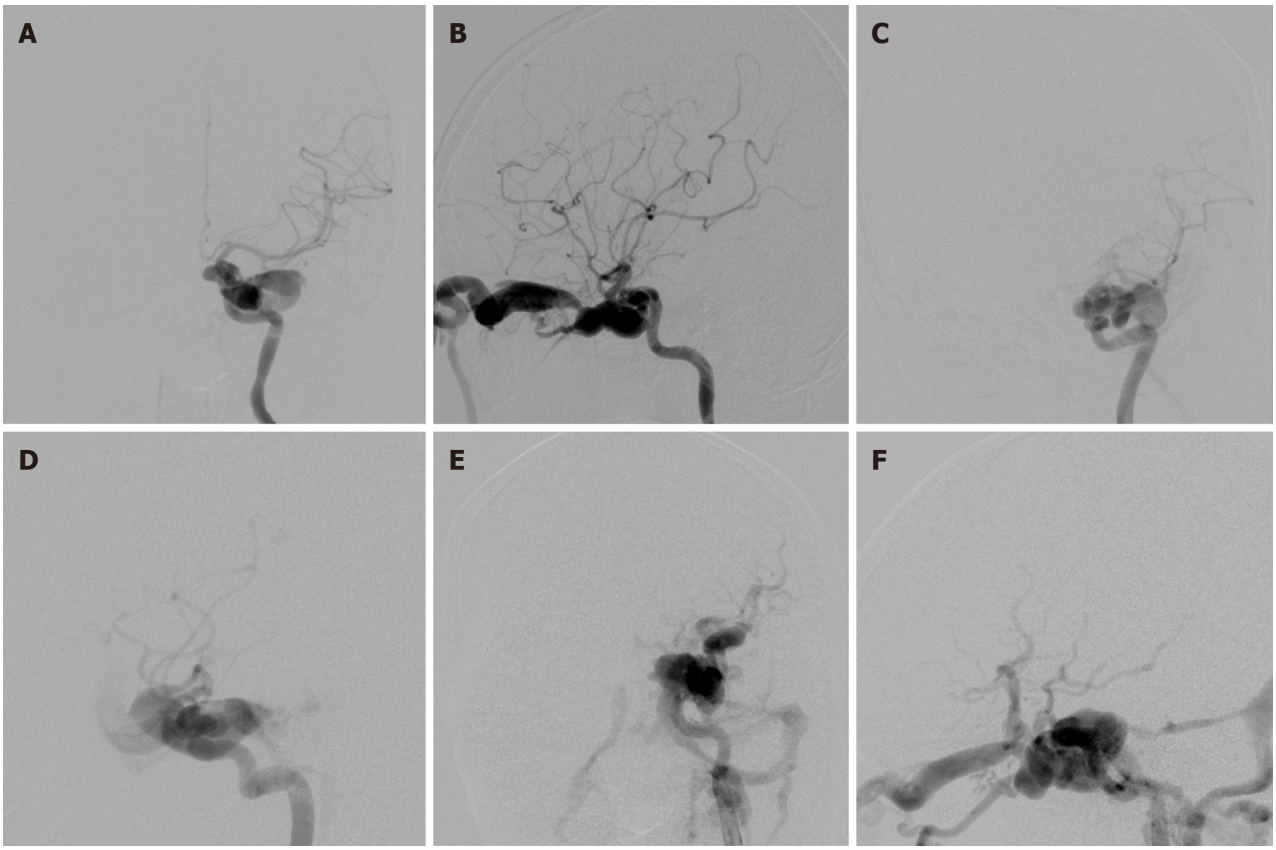

Figure 3 Classification of traumatic carotid-cavernous fistulas according to the fistula size. A and B: Anteroposterior (AP) and lateral views of a small-sized fistula, which had good antegrade ipsilateral internal carotid artery (ICA) flow, represented by opacification of both the anterior cerebral artery (ACA) and middle cerebral artery (MCA); C and D: AP and lateral views of a medium-sized fistula, which had fair antegrade flow, represented by opacification of either the ACA or MCA; E and F: AP and lateral views of a large-sized fistula, which had poor antegrade flow, represented by opacification of neither the ACA nor MCA.

Fistula characteristics

The cohort consisted of 79 fistulas including 14 (17.7%) small, 31 (39.2%) medium, and 34 (43.1%) large fistulas. Fistula locations were right-sided in 40 cases (50.6%) and left-sided in 39 cases (49.4%). The orifice of the fistula was located at C1 in 1 patient (1.3%), C2 in 7 patients (8.9%), C3 in 26 patients (32.9%), C4 in 25 patients (31.6%), and C5 in 20 patients (25.3%).

Treatment outcomes

Treatment outcomes, detailed in Table 2, showed complete obliteration of the fistula in 78 patients (98.8%) and nearly complete obliteration in 1 patient (1.3%). One balloon was used in 51 patients (64.6%), two balloons in 20 patients (25.3%), and three balloons in 8 patients (10.1%). Recurrent fistulas occurred in 13 patients (16.5%; Figures 5 and 6). Parent artery occlusion after treatment or during follow-up was observed in 6 patients (7.6%).

Pseudoaneurysm formation and regression

During a follow-up period of 2-10 years, grade 0 pseudoaneurysm were detected at final CTA follow-up in 24 patients (32.9%), grade 1 in 22 patients (30.1%), grade 2 in 18 patients (24.7%), and grade 3 in 9 patients (12.3%). There were no grade 4 or giant pseudoaneurysms in our study. Spontaneous regression of pseudoaneurysm size occurred in 10 patients (13.7%), with no progression in size observed. Most large pseudoaneurysms developed calcifications around the aneurysmal wall during follow-up at 5 years to 10 years (Figure 7). All patients harboring pseudoaneurysms were asymptomatic during long-term follow-up.

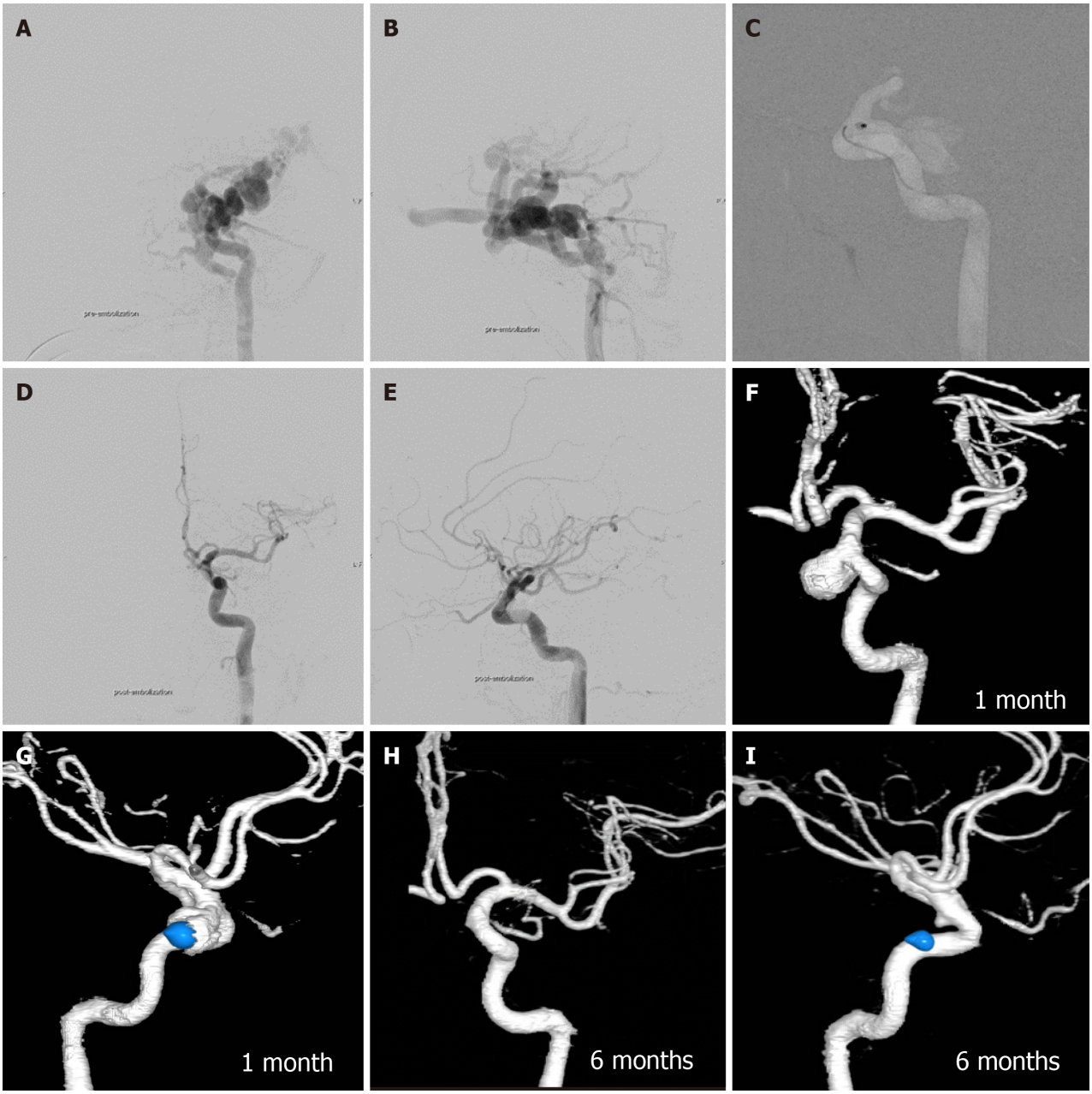

Figure 4 A 22-year-old male presented with left proptosis and red eye after a motor vehicle accident 3 years prior. A and B: Anteroposterior (AP) and lateral views of the left internal carotid artery (LICA) injection showed large traumatic carotid-cavernous fistula without antegrade flow into anterior and middle cerebral arteries; C: Lateral view of the LICA demonstrated a detachable balloon navigating into the orifice of the fistula at the C1 cavernous segment of the LICA under road-mapping; D and E: AP and lateral views of the LICA injection revealed complete obliteration of the fistula after the detachment of the balloon; F and G: AP and lateral views of three-dimensional reconstructed images of the LICA using computed tomography angiography (CTA) obtained 1 month after embolization showed a large pseudoaneurysm (grade 3); H and I: The same projection of the three-dimensional reconstructed images of the LICA using CTA obtained 6 months after embolization demonstrated a minimal residual pseudoaneurysm (grade 1).

Risk factors for pseudoaneurysm formation

Univariate analysis indicated that sex, age, size, location of fistula, and number of balloons used were not related to the occurrence of pseudoaneurysm. The main factor for pseudoaneurysm formation was the size of the balloon including the use of balloon SP (P = 0.005) and balloon No. 6 (P = 0.002; Table 3). The use of balloon SP was associated with higher rates of complete obliteration of fistula without pseudoaneurysm formation, whereas balloon No. 6 developed large-sized pseudoaneurysms compared with other sizes.

Complications related to balloon embolization

Other balloon-related complications were found in 4 patients. Early detachment and migration of the detachable balloon occurred in 1 patient, but the balloon fragment was successfully retrieved with a snare without further ischemic symptoms. Three patients developed transient oculomotor nerve palsy after balloon embolization.

Table 3 Comparison of balloon size and pseudoaneurysm grade, *n* (%)

Balloon size	Pseudoaneurysm grade				*P* value
	0	1	2	3	
No. 4	1 (16.7)	4 (66.6)	1 (16.7)	0 (0.0)	0.348
No. 5	2 (13.3)	7 (46.7)	4 (26.7)	2 (13.3)	0.233
No. 6	2 (15.4)	2 (15.4)	3 (23.1)	6 (46.1)	0.002[a]
SP	19 (44.2)	12 (27.9)	11 (25.6)	1 (2.3)	0.005[a]

[a]$P < 0.05$.

DISCUSSION

The goal of treatment of TCCF using a detachable balloon is to occlude the fistula while maintaining the carotid flow by the balloon placed into the cavernous sinus (venous side)[23,24]. In our study, we compared therapeutic outcomes of patients with TCCFs treated with transarterial detachable balloon embolization from different centers as shown in Table 4 [12-14,19-22,25-32]. Two principal complications identified in balloon embolization for TCCF are the recurrence of the fistula and the formation of a pseudoaneurysm. Numerous studies have explored and identified risk factors contributing to the recurrence of TCCF following balloon embolization[21,29,32]. However, our study primarily concentrated on investigating the relevant factors associated with the occurrence of pseudoaneurysm, as this aspect has been less extensively covered in the existing literature.

Detachable latex and silicone balloon

Materials for the detachable balloons are made of either natural rubber (latex) or silicone rubber[31]. Under an electron microscope, the silicone detachable balloons display a smooth surface, whereas latex balloons exhibit an irregular surface with numerous large deep craters. These surface irregularities in latex balloons cause turbulent flow, promoting thrombosis and a more pronounced inflammatory response. Consequently, latex balloons are more thrombogenic than their silicone counterparts[30,33]. *In vivo*, if the tail of latex balloons protruded into the parent artery, it may increase thrombus formation around the balloons, more likely leading to parent artery occlusion as found in 7.6% of our patients [34]. Latex balloons are less expensive than silicone balloons and offer greater elasticity, allowing for larger inflation sizes. Detachable latex balloons can be more firmly attached to delivery catheters than silicone balloons and therefore should offer appreciably less risk of premature detachment. Latex balloons have a variety of sizes and shapes and require a hand ligation attachment, and they were reported as more prone to early deflation[27].

Silicone balloons are softer than latex and tend to conform to the shape of the vessel or aneurysm, reducing the risk of vessel rupture. Silicone balloons are also biocompatible, with their shell not degrading over time inside the vessel unlike latex[35]. Detachable silicone balloons are semipermeable and must be inflated with isotonic solutions. To prevent early deflation of the balloon, detachable silicone balloons require filling with iso-osmolar iodinated contrast agent before detachment[36-38]. On the other hand, latex balloons are not semipermeable, so the osmotic gradient between the balloon contents and the surrounding plasma has no influence on the role of premature deflation[39,40].

Balloons can be inflated with polymerizing substances, such as hydroxyethyl methacrylate, silicone fluid, or iodinated contrast material. A balloon filled with a polymerizing substance will produce better anatomic results and reduce the occurrence of a pseudoaneurysm. But the polymerizing substance may result in poor or incomplete recovery from oculomotor nerve palsy due to the remaining permanently solid balloon. In contrast, an iodine-inflated balloon may progressively deflate, possibly causing a pseudoaneurysm. However, when oculomotor nerve palsy occurs, balloon deflation will usually result in complete recovery from the palsy[24,28,31]. Currently, detachable silicone balloons are not available, and detachable latex balloons have been used by inflating with iodinated contrast material.

Pseudoaneurysm formation following transarterial balloon embolization

Pseudoaneurysms are remnants of the wall defect of the cavernous ICA at the orifice of the fistula that form following early deflation or migration of the detachable balloon[26,41]. The balloons usually become progressively deflated in 3 wk or 4 wk[10]. It is crucial for the balloons to stay inflated or retain their size and shape for approximately 2 wk to ensure a secure fibrous attachment to the vascular wall[11]. Premature deflation of the balloon often leads to the recurrence of fistulas and the subsequent development of pseudoaneurysms[14]. Balloons that deflate too early tend to migrate forward, ending up retained in the cavernous sinus[29]. The early deflation of balloons is caused primarily by relaxation or insufficiency of the ligature[10,12,20].

According to our review (Table 4), the incidence of pseudoaneurysm formation ranges from 2.4% to 44.0%. To our knowledge, there has been no study focusing on the long-term follow-up of pseudoaneurysm post-transarterial balloon embolization in TCCF. Our study found the highest incidence of pseudoaneurysm formation at 67.1%, including small-sized pseudoaneurysms in 30.1% of cases, medium-sized in 24.7%, and large-sized in 12.3%. The size of pseudoaneurysm spontaneously regressed in 13.7% during follow-up CTA, and there was no progression of pseudoaneurysms in our series. Interestingly, most large pseudoaneurysms developed rim calcification during follow-up at 5 years to 10 years.

Table 4 Comparative therapeutic outcomes in patients harboring traumatic carotid-cavernous fistula treated with transarterial detachable balloon embolization from different centers

Ref.	Total cases	Total fistula treated with DB	Balloon type	Preservation of ICA (%)	Recurrence (%)	Pseudoaneurysm (%)	Other balloon-related complications (*n*)
Debrun *et al*[12], 1981	54	54	Latex	59.0	9.3	44.0	Transient oculomotor nerve palsy (11)
Tsai *et al*[13], 1983	58	43	Latex	N/A	2.3	32.5	Migration of deflated balloon into the ICA (2); delayed stroke (1)
Berthelsen and Svendsen[14], 1987	14	10	Latex	N/A	21.4	N/A	Transient ischemic attack (1); migration of balloon into MCA (1)
Higashida *et al*[26], 1989	206	206	Silicone	88.0	0	2.4	Oculomotor nerve palsy (1); ischemic stroke (5)
Lewis *et al*[27], 1995	100	88	Latex/Silicone	75.0	5.7	N/A	Transient ischemia episodes (3); death (1)
Wu *et al*[28], 2000	482	471	Latex	84.0	3.3	N/A	Cerebral infarction (2); vision loss (1)
Luo *et al*[29], 2004	143	143	Latex	81.0	11.2	N/A	N/A
Szkup and Beningfield[30], 2005	34	34	Latex	53.0	N/A	N/A	Transient hemiparesis (1)
Gupta *et al*[31], 2006	89	79	Latex	98.0	0	N/A	Transient cranial palsy (1)
Wang *et al*[22], 2011	51	44	Latex	85.0	11.4	18.2	None
Malan *et al*[25], 2012	32	17	Latex	66.0	15.6	N/A	Balloon displacement (3); balloon rupture or deflation (8)
Xu *et al*[32], 2013	58	58	Latex	87.9	12.1	N/A	None
Chi *et al*[20], 2014	172	138	Latex	70.0	9.8	N/A	Transient hemiparesis (1); transient oculomotor nerve palsy (1); vagal shock, death (1)
Gao *et al*[21], 2018	188	182	Latex	85.7	13.9	N/A	Cerebral embolism (1); abducent nerve paralysis (2)
Niu *et al*[19], 2020	24	21	Latex	90.4	8.3	4.2	Oculomotor and abducens nerve palsy (1); abducens nerve palsy (1)
Present study	79	79	Latex	92.4	16.5	67.1	Early detachment and migration of balloon (1); transient oculomotor nerve palsy (3)

DB: Detachable balloon; ICA: Internal carotid artery; N/A: Data not applicable; TCCF: Traumatic carotid-cavernous fistula; MCA: Middle cerebral artery.

Impact of detachable latex balloon size on pseudoaneurysm formation

Currently, GOLDBAL is the only detachable latex balloon available in our institute. Its deployment requires a single microcatheter, and the balloon is secured over a coaxial microcatheter using a latex thread. This thread then forms a self-sealing valve when the balloon is detached. Proper preparation and deployment of this system demands significant experience and skill[36,42].

In our study, univariate analysis showed that factors such as sex, age, fistula size and location, and the number of balloons used were not significant contributors in pseudoaneurysm development. Instead, the main contributing factor was the size of the balloon, specifically the use of balloon SP ($P = 0.005$) and balloon No. 6 ($P = 0.002$). The SP balloon was linked to higher rates of complete fistula obliteration without pseudoaneurysm formation, while the balloon No. 6 was associated with the development of large pseudoaneurysms.

Detachable balloon SP and No. 6 have different shapes and sizes. The balloon SP is spherical, holding a maximum volume of 0.9 mL, and expands to dimensions of 12 mm × 13 mm when fully inflated. In contrast, the balloon No. 6 is cylindrical, with a maximum volume of 3 mL, and expands to 15 mm × 25 mm. Detachable balloon No. 6 is the largest size and the most difficult to advance through a 9 F guiding catheter with some friction. We speculate that the ligature might relax, or the balloon may be damaged during prolonged manipulation, leading to early deflation and the formation

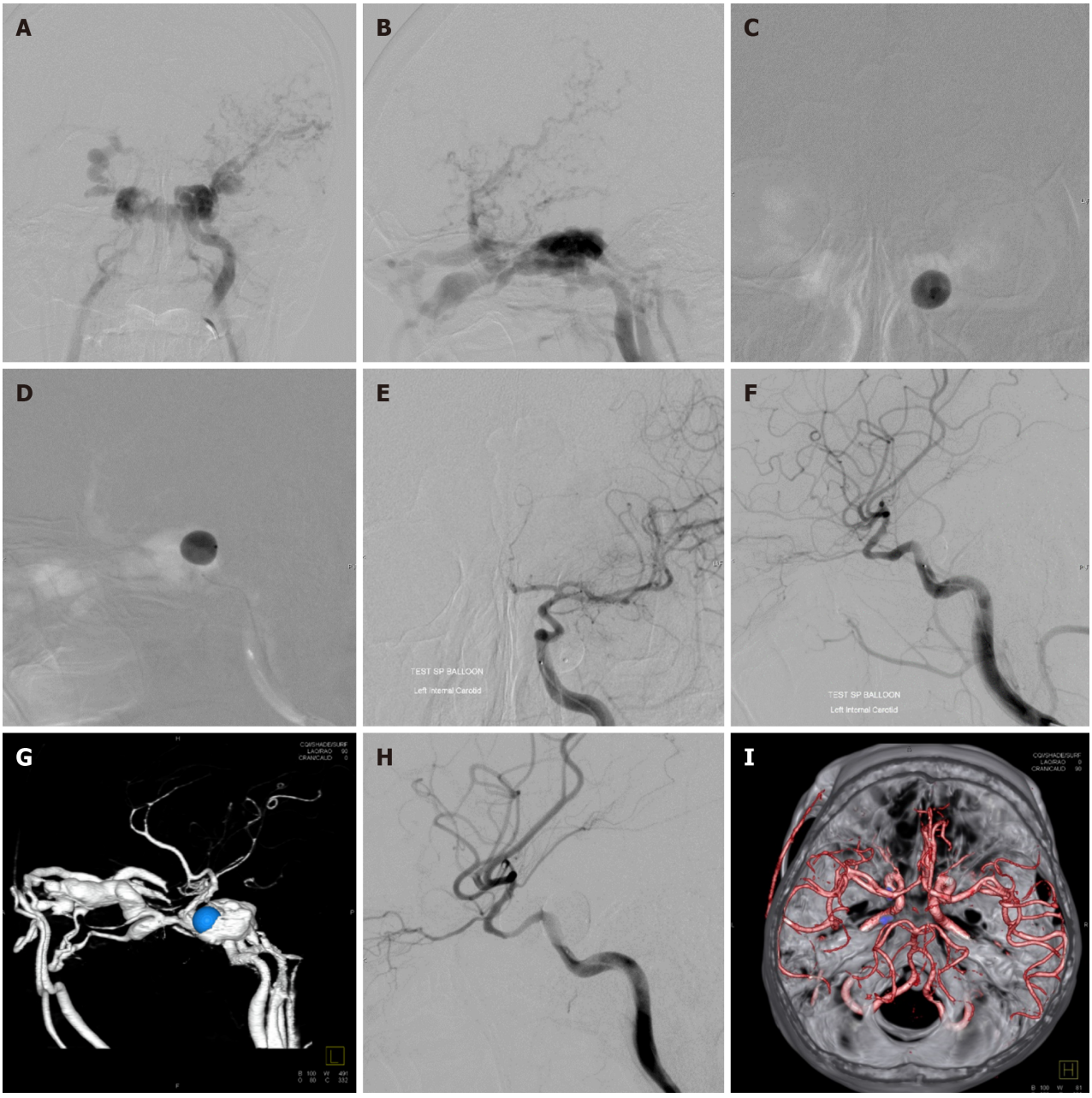

Figure 5 A 40-year-old male presented with left proptosis and audible bruit after a motor vehicle accident 4 months prior. A and B: Anteroposterior (AP) and lateral views of the left internal carotid artery (LICA) injection showed large traumatic carotid-cavernous fistula without antegrade flow into the anterior and middle cerebral arteries; C and D: AP and lateral views of the LICA demonstrated a detachable balloon during inflation at the left posterior cavernous sinus under road-mapping; E and F: AP and lateral views of the LICA injection revealed complete obliteration of the fistula; G: Lateral view of three-dimensional reconstructed images of the LICA using computed tomography angiography (CTA) of the LICA obtained 3 d after embolization showed recurrent traumatic carotid-cavernous fistula with displacement of a balloon into the anterior cavernous sinus; H: Lateral view of the LICA injection revealed complete obliteration of the fistula after retreatment with another balloon; I: Three-dimensional reconstructed image of both ICAs, vertebrobasilar system, and skull base using CTA obtained 6 months after embolization confirmed no residual pseudoaneurysm (grade 0).

of large pseudoaneurysms.

Recent advances in coil and flow divertor technologies have significantly impacted the treatment of intracranial aneurysms. In contrast, the development of detachable balloons, specifically latex detachable balloons, has not had similar progress. Although not approved by the Food and Drug Administration for use in the United States, these balloons are utilized in certain Southeast Asian countries, reflecting regional differences in medical practice and regulation. The market for detachable latex balloons is notably small, leading to a decrease in their manufacturing[36]. Despite this, detachable balloons maintain a role in treating TCCF and occluding vessels. It is anticipated that future developments in detachable balloon technology could potentially address current limitations, such as the risk of pseudoaneurysm formation, thereby enhancing the efficacy and safety of these devices in clinical practice.

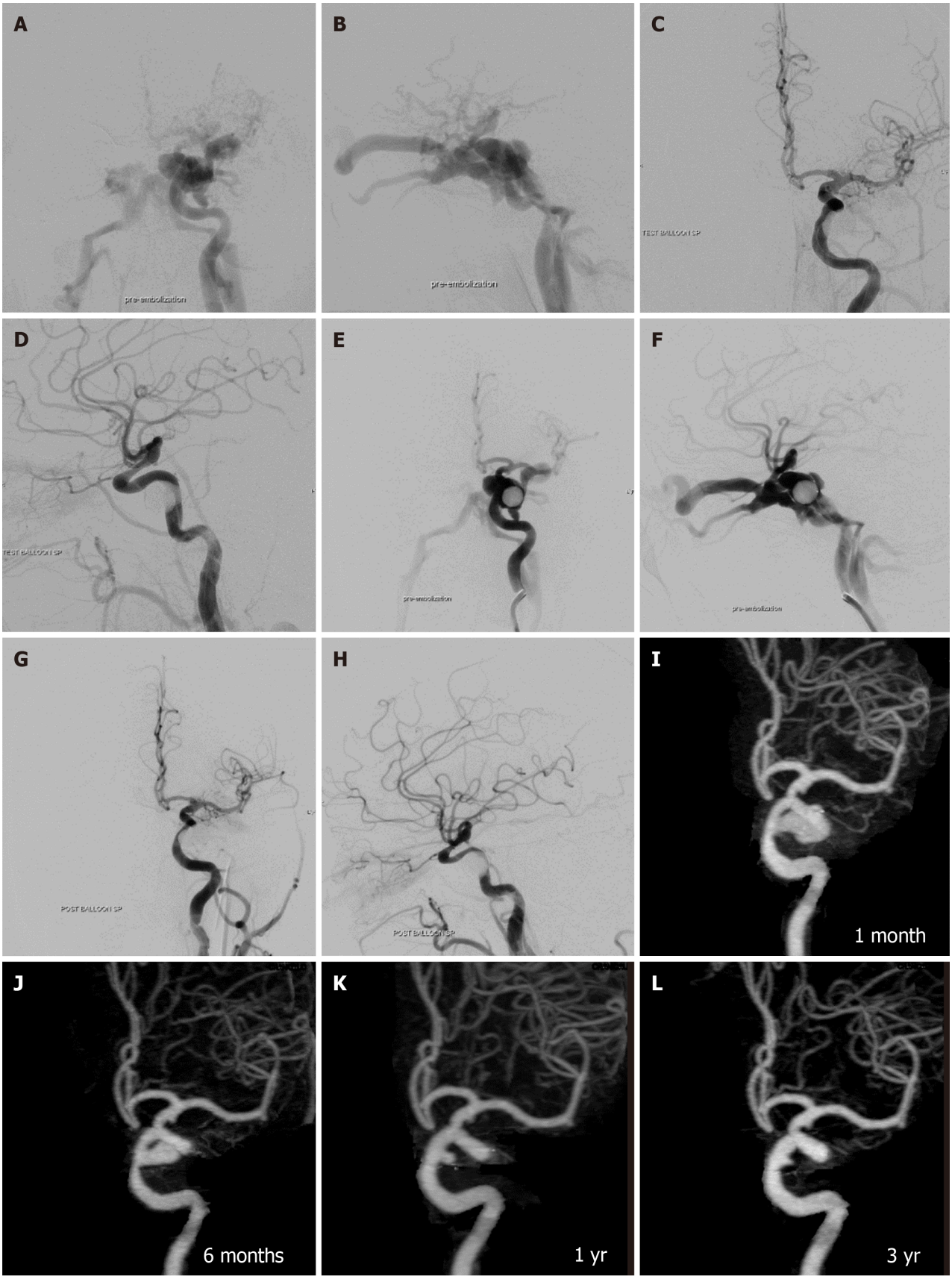

Figure 6 A 27-year-old male presented with left proptosis and red eye immediately after a motor vehicle accident. A and B: Anteroposterior (AP) and lateral views of the left internal carotid artery (LICA) injection showed large traumatic carotid-cavernous fistula without antegrade flow into the anterior and middle cerebral arteries; C and D: AP and lateral views of the LICA revealed complete obliteration of the fistula after the detachment of the balloon; E and F: AP and lateral views of the LICA obtained 1 wk later demonstrated recurrent traumatic carotid-cavernous fistula; G and H: AP and lateral views of the LICA confirmed complete obliteration after retreatment with balloon embolization; I-L: AP views of the three-dimensional reconstructed images of the LICA using computed

tomography angiography at 1 month (I), 6 months (J), 1 year (K), and 3 years (L) on the same projection demonstrated the regression of pseudoaneurysm at C5 cavernous segment of the LICA from large (grade 3) to small (grade 1) size.

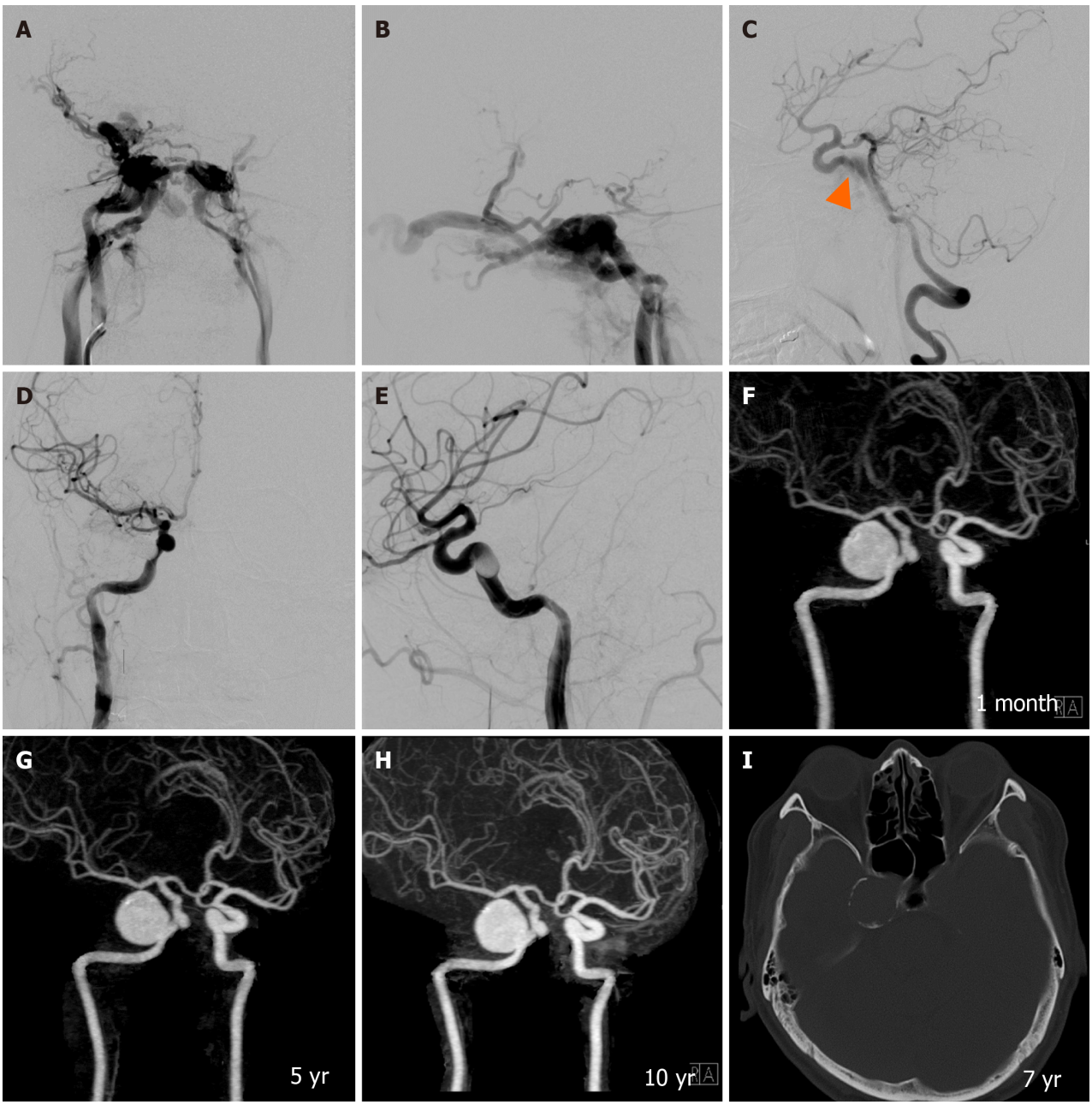

Figure 7 A 30-year-old male presented with right proptosis and red eye 1 d following a motor vehicle accident. A and B: Anteroposterior (AP) and lateral views of the right internal carotid artery (RICA) injection showed large traumatic carotid-cavernous fistula without antegrade flow into the anterior and middle cerebral arteries; C: Lateral view of the right vertebral artery with compression of the cervical carotid artery demonstrated the fistula (arrowhead) at the C5 cavernous segment of the RICA; D and E: AP and lateral views of the RICA confirmed complete obliteration of the fistula after the detachment of the balloon; F-H: Oblique views of three-dimensional reconstructed images of both ICAs using computed tomography angiography (CTA) at 1 month (F), 5 years (G), and 10 years (H) on the same projection revealed a large pseudoaneurysm (grade 3) measuring 20 mm × 20 mm × 23 mm in size; I: Axial view of bone-window ICA scan obtained 7 years after balloon embolization showed peripheral rim calcification around the aneurysmal wall.

Management of pseudoaneurysms occurring after detachable balloon embolization

Pseudoaneurysms, following the treatment of TCCF with detachable balloons, may either enlarge, causing a mass effect, or remain asymptomatic and decrease in size. The incidence of clinically symptomatic pseudoaneurysms is relatively low [13]. Small pseudoaneurysms typically remain asymptomatic and stable in size, while larger pseudoaneurysms can cause symptoms such as cranial nerve palsy and severe retroorbital pain[14,24,41]. Spontaneous regression of pseudoaneurysms after detachable balloon occlusion of TCCF has rarely been reported[43].

In most cases, pseudoaneurysms tend to be asymptomatic and do not necessitate further intervention[12]. However, some authors have suggested more aggressive treatment due to potential complications, which include mass effect on adjacent structures, recurrent TCCF from rupture of the pseudoaneurysm, and cerebral embolism resulting from thrombus formation[22].

For large symptomatic pseudoaneurysms, treatment options may include permanent occlusion of the carotid artery or the use of covered stents to preserve the integrity of the ICA[12,22,24]. In selected patients, pseudoaneurysms can be safely and effectively treated by embolization with detachable coils[44]. In our study, all patients with pseudoaneurysms remained asymptomatic, and no additional therapy was required during the long-term follow-up.

CONCLUSION

Our study showed that pseudoaneurysm formation was a common complication of detachable balloon embolization for treatment of TCCF. The main risk factor influencing this outcome was identified as the size of the detachable balloon used in treatment. Specifically, the balloon SP was associated with a higher success rate in completely obliterating the fistula without leading to the formation of pseudoaneurysms. In contrast, the largest balloon, No. 6, was more prone to result in the development of large-sized pseudoaneurysms. We speculate that the ligature might relax or the balloon may be damaged during prolonged manipulation, leading to early deflation and the formation of large pseudoaneurysms. Despite the high incidence of pseudoaneurysm formation, it is noteworthy that all patients with pseudoaneurysms remained asymptomatic throughout the long-term follow-up period. This observation underscores the complexity of managing TCCF and the need for careful consideration of the tools and techniques employed in treatment.

FOOTNOTES

Author contributions: Iampreechakul P proposed the study concept and design; Iampreechakul P and Siriwimonmas S contributed to the manuscript writing; Wangtanaphat K, Chuntaroj S, and Lertbutsayanukul P contributed to data acquisition; Wattanasen Y and Hangsapruek S contributed to data analysis and interpretation; Puthkhao P contributed to statistical analysis; Iampreechakul P and Puthkhao P contributed to manuscript revision.

Institutional review board statement: The study was approved by the Neurological Institute of Thailand Institutional Review Board (No. 54020).

Informed consent statement: Patients were not required to give informed consent to the study because the analysis used anonymized clinical data that were obtained after each patient agreed to treatment by written consent.

Conflict-of-interest statement: The authors declare having no conflicts of interest.

Data sharing statement: The data used to support the findings to this study are available from the corresponding author upon request.

ORCID number: Prasert Iampreechakul 0000-0002-8241-7955; Korrapakc Wangtanaphat 0000-0001-5775-6296; Songpol Chuntaroj 0000-0001-6282-3908; Yodkhwan Wattanasen 0000-0002-3348-1264; Sunisa Hangsapruek 0000-0003-3229-8131; Punjama Lertbutsayanukul 0000-0002-0912-5868; Pimchanok Puthkhao 0000-0001-6167-0292; Somkiet Siriwimonmas 0000-0003-0575-4808.

S-Editor: Lin C
L-Editor: A
P-Editor: Zhao S

REFERENCES

1 **Iampreechakul P**, Wangtanaphat K, Lertbutsayanukul P, Siriwimonmas S. Revascularization of the internal carotid artery through the hypertrophied vasa vasorum in traumatic carotid-cavernous fistula previously treated by ligation of cervical carotid arteries: A case report. *Surg Neurol Int* 2022; **13**: 324 [PMID: 36128096 DOI: 10.25259/SNI_450_2022]

2 **Barrow DL**, Spector RH, Braun IF, Landman JA, Tindall SC, Tindall GT. Classification and treatment of spontaneous carotid-cavernous sinus fistulas. *J Neurosurg* 1985; **62**: 248-256 [PMID: 3968564 DOI: 10.3171/jns.1985.62.2.0248]

3 **Iampreechakul P**, Tirakotai W, Tanpun A, Wattanasen Y, Lertbusayanukul P, Siriwimonmas S. Spontaneous resolution of direct carotid-cavernous fistulas: case series and literature review. *Interv Neuroradiol* 2019; **25**: 71-89 [PMID: 30244626 DOI: 10.1177/1591019918800220]

4 **Iampreechakul P**, Tanpun A, Lertbusayanukul P, Siriwimonmas S. Contralateral extensive cerebral hemorrhagic venous infarction caused by retrograde venous reflux into the opposite basal vein of Rosenthal in posttraumatic carotid-cavernous fistula: A case report and literature

review. *Interv Neuroradiol* 2018; **24**: 546-558 [PMID: 29781369 DOI: 10.1177/1591019918776615]

5 **Iampreechakul P**, Liengudom A, Tirakotai W, Wangtanaphat K, Lertbutsayanukul P, Hangsapruek S, Siriwimonmas S. Combined endovascular and microsurgical management of complex traumatic carotid-cavernous fistula: Three case reports. *Surg Neurol Int* 2022; **13**: 337 [PMID: 36128157 DOI: 10.25259/SNI_308_2022]

6 **Prolo DJ**, Hanbery JW. Intraluminal occlusion of a carotid-cavernous sinus fistula with a balloon catheter. Technical note. *J Neurosurg* 1971; **35**: 237-242 [PMID: 5570787 DOI: 10.3171/jns.1971.35.2.0237]

7 **Serbinenko FA**. Balloon catheterization and occlusion of major cerebral vessels. *J Neurosurg* 1974; **41**: 125-145 [PMID: 4841872 DOI: 10.3171/jns.1974.41.2.0125]

8 **Debrun G**, Lacour P, Caron JP, Hurth M, Comoy J, Keravel Y. Inflatable and released balloon technique experimentation in dog -- application in man. *Neuroradiology* 1975; **9**: 267-271 [PMID: 1165852 DOI: 10.1007/bf00333741]

9 **Debrun G**, Lacour P, Caron JP, Hurth M, Comoy J, Kéravel Y, Loisance D. [Treatment of arteriovenous fistulas and of aneurysms using an inflatable and releasable balloon. Experimental principles. Application to man]. *Nouv Presse Med* 1975; **4**: 2315-2318 [PMID: 1101212]

10 **Debrun G**, Lacour P, Caron JP, Hurth M, Comoy J, Keravel Y. Detachable balloon and calibrated-leak balloon techniques in the treatment of cerebral vascular lesions. *J Neurosurg* 1978; **49**: 635-649 [PMID: 712387 DOI: 10.3171/jns.1978.49.5.0635]

11 **Leipzig TJ**, Mullan SF. Deflation of metrizamide-filled balloon used to occlude a carotid-cavernous fistula. Case report. *J Neurosurg* 1983; **59**: 524-528 [PMID: 6224917 DOI: 10.3171/jns.1983.59.3.0524]

12 **Debrun G**, Lacour P, Vinuela F, Fox A, Drake CG, Caron JP. Treatment of 54 traumatic carotid-cavernous fistulas. *J Neurosurg* 1981; **55**: 678-692 [PMID: 6458669 DOI: 10.3171/jns.1981.55.5.0678]

13 **Tsai FY**, Hieshima GB, Mehringer CM, Grinnell V, Pribram HW. Delayed effects in the treatment of carotid-cavernous fistulas. *AJNR Am J Neuroradiol* 1983; **4**: 357-361 [PMID: 6410744]

14 **Berthelsen B**, Svendsen P. Treatment of direct carotid-cavernous fistulas with detachable balloons. *Acta Radiol* 1987; **28**: 683-691 [PMID: 2962600 DOI: 10.3109/02841858709177424]

15 **Barrow DL**, Fleischer AS, Hoffman JC. Complications of detachable balloon catheter technique in the treatment of traumatic intracranial arteriovenous fistulas. *J Neurosurg* 1982; **56**: 396-403 [PMID: 7057237 DOI: 10.3171/jns.1982.56.3.0396]

16 **Chalif DJ**, Flamm ES, Berenstein A, Choi IS. Microsurgical removal of a balloon embolus to the internal carotid artery. Case report. *J Neurosurg* 1983; **58**: 112-116 [PMID: 6336626 DOI: 10.3171/jns.1983.58.1.0112]

17 **Graeb DA**, Robertson WD, Lapointe JS, Nugent RA. Avoiding intraarterial balloon detachment in the treatment of posttraumatic carotid-cavernous fistulae with detachable balloons. *AJNR Am J Neuroradiol* 1985; **6**: 602-605 [PMID: 3927679]

18 **Ducruet AF**, Albuquerque FC, Crowley RW, McDougall CG. The evolution of endovascular treatment of carotid cavernous fistulas: a single-center experience. *World Neurosurg* 2013; **80**: 538-548 [PMID: 23402868 DOI: 10.1016/j.wneu.2013.02.033]

19 **Niu Y**, Chen T, Tang J, Jiang Z, Zhu G, Chen Z. Detachable balloon embolization as the preferred treatment option for traumatic carotid-cavernous sinus fistula? *Interv Neuroradiol* 2020; **26**: 90-98 [PMID: 31451026 DOI: 10.1177/1591019919871849]

20 **Chi CT**, Nguyen D, Duc VT, Chau HH, Son VT. Direct traumatic carotid cavernous fistula: angiographic classification and treatment strategies. Study of 172 cases. *Interv Neuroradiol* 2014; **20**: 461-475 [PMID: 25207910 DOI: 10.15274/inr-2014-10020]

21 **Gao BL**, Wang ZL, Li TX, Xu B. Recurrence risk factors in detachable balloon embolization of traumatic direct carotid cavernous fistulas in 188 patients. *J Neurointerv Surg* 2018; **10**: 704-707 [PMID: 29021309 DOI: 10.1136/neurintsurg-2017-013384]

22 **Wang W**, Li YD, Li MH, Tan HQ, Gu BX, Wang J, Zhang PL. Endovascular treatment of post-traumatic direct carotid-cavernous fistulas: A single-center experience. *J Clin Neurosci* 2011; **18**: 24-28 [PMID: 20888773 DOI: 10.1016/j.jocn.2010.06.008]

23 **Debrun GM**. Treatment of traumatic carotid-cavernous fistula using detachable balloon catheters. *AJNR Am J Neuroradiol* 1983; **4**: 355-356 [PMID: 6410743]

24 **Sbeih IA**, O'Laoire SA. Traumatic carotid-cavernous fistula due to transection of the intracavernous carotid artery. Case report. *J Neurosurg* 1984; **60**: 1080-1084 [PMID: 6716143 DOI: 10.3171/jns.1984.60.5.1080]

25 **Malan J**, Lefeuvre D, Mngomezulu V, Taylor A. Angioarchitecture and treatment modalities in posttraumatic carotid cavernous fistulae. *Interv Neuroradiol* 2012; **18**: 178-186 [PMID: 22681733 DOI: 10.1177/159101991201800209]

26 **Higashida RT**, Halbach VV, Tsai FY, Norman D, Pribram HF, Mehringer CM, Hieshima GB. Interventional neurovascular treatment of traumatic carotid and vertebral artery lesions: results in 234 cases. *AJR Am J Roentgenol* 1989; **153**: 577-582 [PMID: 2763958 DOI: 10.2214/ajr.153.3.577]

27 **Lewis AI**, Tomsick TA, Tew JM Jr. Management of 100 consecutive direct carotid-cavernous fistulas: results of treatment with detachable balloons. *Neurosurgery* 1995; **36**: 239-44; discussion 244 [PMID: 7731502 DOI: 10.1227/00006123-199502000-00001]

28 **Wu Z**, Zhang Y, Wang C, Yang X, Li Y. Treatment of traumatic carotid-cavernous fistula. *Interv Neuroradiol* 2000; **6**: 277-289 [PMID: 20667206 DOI: 10.1177/159101990000600402]

29 **Luo CB**, Teng MM, Yen DH, Chang FC, Lirng JF, Chang CY. Endovascular embolization of recurrent traumatic carotid-cavernous fistulas managed previously with detachable balloons. *J Trauma* 2004; **56**: 1214-1220 [PMID: 15211128 DOI: 10.1097/01.ta.0000131213.93205.57]

30 **Szkup P**, Beningfield S. Endovascular treatment of post-traumatic carotid-cavernous fistulae using latex detachable balloons. *S Afr J Radiol* 2005; **9**: 4 [DOI: 10.4102/sajr.v9i1.90]

31 **Gupta AK**, Purkayastha S, Krishnamoorthy T, Bodhey NK, Kapilamoorthy TR, Kesavadas C, Thomas B. Endovascular treatment of direct carotid cavernous fistulae: a pictorial review. *Neuroradiology* 2006; **48**: 831-839 [PMID: 16969673 DOI: 10.1007/s00234-006-0132-x]

32 **Xu XQ**, Liu S, Zu QQ, Zhao LB, Xia JG, Zhou CG, Zhou WZ, Shi HB. Follow-up of 58 traumatic carotid-cavernous fistulas after endovascular detachable-balloon embolization at a single center. *J Clin Neurol* 2013; **9**: 83-90 [PMID: 23626645 DOI: 10.3988/jcn.2013.9.2.83]

33 **Heilman CB**, Kwan ES, Wu JK. Aneurysm recurrence following endovascular balloon occlusion. *J Neurosurg* 1992; **77**: 260-264 [PMID: 1625015 DOI: 10.3171/jns.1992.77.2.0260]

34 **Miyachi S**, Negoro M, Handa T, Terashima K, Keino H, Sugita K. Histopathological study of balloon embolization: silicone versus latex. *Neurosurgery* 1992; **30**: 483-489 [PMID: 1584344 DOI: 10.1227/00006123-199204000-00002]

35 **Higashida RT**, Halbach VV, Dowd C, Barnwell SL, Dormandy B, Bell J, Hieshima GB. Endovascular detachable balloon embolization therapy of cavernous carotid artery aneurysms: results in 87 cases. *J Neurosurg* 1990; **72**: 857-863 [PMID: 2338569 DOI: 10.3171/jns.1990.72.6.0857]

36 **Alaraj A**, Wallace A, Dashti R, Patel P, Aletich V. Balloons in endovascular neurosurgery: history and current applications. *Neurosurgery*

2014; **74** Suppl 1: S163-S190 [PMID: 24402485 DOI: 10.1227/NEU.0000000000000220]

37 **White RI Jr**, Ursic TA, Kaufman SL, Barth KH, Kim W, Gross GS. Therapeutic embolization with detachable balloons. Physical factors influencing permanent occlusion. *Radiology* 1978; **126**: 521-523 [PMID: 622506 DOI: 10.1148/126.2.521]

38 **DiTullio MV Jr**, Rand RW, Frisch E. Detachable balloon catheter. Its application in experimental arteriovenous fistulae. *J Neurosurg* 1978; **48**: 717-723 [PMID: 641551 DOI: 10.3171/jns.1978.48.5.0717]

39 **Tomsick TA**. Osmotic effects upon long term inflation of latex detachable balloons. *Neurosurgery* 1985; **17**: 952-954 [PMID: 4080129 DOI: 10.1227/00006123-198512000-00014]

40 **Hawkins TD**, Szaz KF. The permeability of detachable latex rubber balloons. An in vitro study. *Invest Radiol* 1987; **22**: 969-972 [PMID: 3440732 DOI: 10.1097/00004424-198712000-00010]

41 **Lewis AI**, Tomsick TA, Tew JM Jr, Lawless MA. Long-term results in direct carotid-cavernous fistulas after treatment with detachable balloons. *J Neurosurg* 1996; **84**: 400-404 [PMID: 8609550 DOI: 10.3171/jns.1996.84.3.0400]

42 **Beaujeux RL**, Reizine DC, Casasco A, Aymard A, Rüfenacht D, Khayata MH, Riché MC, Merland JJ. Endovascular treatment of vertebral arteriovenous fistula. *Radiology* 1992; **183**: 361-367 [PMID: 1561336 DOI: 10.1148/radiology.183.2.1561336]

43 **Lee CH**, Kim MS, Lee GJ. Spontaneous Regression of the Pseudoaneurysm Developed after Balloon Occlusion of the Direct Carotid-cavernous Fistula. *J Korean Neurosurg Soc* 2007; **41**: 323-326

44 **Lempert TE**, Halbach VV, Higashida RT, Dowd CF, Urwin RW, Balousek PA, Hieshima GB. Endovascular treatment of pseudoaneurysms with electrolytically detachable coils. *AJNR Am J Neuroradiol* 1998; **19**: 907-911 [PMID: 9613510]

Published by **Baishideng Publishing Group Inc**
7041 Koll Center Parkway, Suite 160, Pleasanton, CA 94566, USA
Telephone: +1-925-3991568
E-mail: office@baishideng.com
Help Desk: https://www.f6publishing.com/helpdesk
https://www.wjgnet.com